

Downstream STING pathways IRF3 and NF- κ B differentially regulate CCL22 in response to cytosolic dsDNA

Jihyun Kim

Department of Biomedical Sciences, Mercer University School of Medicine, Macon, GA, USA

Jocelyn V. Pena

Department of Biomedical Sciences, Mercer University School of Medicine, Macon, GA, USA

Hannah P. McQueen

Department of Biomedical Sciences, Mercer University School of Medicine, Macon, GA, USA

Lingwei Kong

Department of Biomedical Sciences, Mercer University School of Medicine, Macon, GA, USA

Elmira M. Lomashvili

Department of Biomedical Sciences, Mercer University School of Medicine, Macon, GA, USA

Dina Michael

Department of Biomedical Sciences, Mercer University School of Medicine, Macon, GA, USA

Pamela R. Cook (✉ cook_p@mercer.edu)

Department of Biomedical Sciences, Mercer University School of Medicine, Macon, GA, USA

Article

Keywords: CCL22, dsDNA, IRF3, STING, oncolytic viruses, DNA cancer vaccines, STING agonists, transposable elements

Posted Date: November 30th, 2022

DOI: <https://doi.org/10.21203/rs.3.rs-2264736/v1>

License: © ⓘ This work is licensed under a Creative Commons Attribution 4.0 International License.

[Read Full License](#)

Additional Declarations: There is **NO** conflict of interest to disclose.

Version of Record: A version of this preprint was published at Cancer Gene Therapy on November 21st, 2023. See the published version at <https://doi.org/10.1038/s41417-023-00678-z>.

Abstract

Double-stranded DNA (dsDNA) in the cytoplasm of eukaryotic cells is abnormal and typically indicates the presence of pathogens or mislocalized self-DNA. Multiple sensors detect cytosolic dsDNA and trigger robust immune responses via activation of type I interferons. Several cancer immunotherapy treatments also activate cytosolic nucleic acid sensing pathways, including oncolytic viruses, nucleic acid-based cancer vaccines, and pharmacological agonists. We report here that cytosolic dsDNA introduced into malignant cells can robustly upregulate expression of CCL22, a chemokine responsible for the recruitment of regulatory T cells (Tregs). Tregs in the tumor microenvironment are thought to repress anti-tumor immune responses and contribute to tumor immune evasion. Surprisingly, we found that CCL22 upregulation by dsDNA was mediated primarily by interferon regulatory factor 3 (IRF3), a key transcription factor that activates type I interferons. This finding was unexpected given previous reports that type I interferon alpha inhibits CCL22 and that IRF3 is associated with strong anti-tumor immune responses, not Treg recruitment. We also found that CCL22 upregulation by dsDNA occurred concurrently with IFN- β upregulation. IRF3 is one of two transcription factors downstream of the STimulator of INterferon Genes (STING), which is a hub adaptor protein through which many different dsDNA sensors transmit their signals. The other transcription factor downstream of STING, NF- κ B, has been reported to regulate CCL22 expression in other contexts, and NF- κ B has been ascribed multiple pro-tumor functions, including Treg recruitment. However, we found that NF- κ B in the context of activation by cytosolic dsDNA contributed minimally to CCL22 upregulation compared with IRF3. Lastly, we observed that two strains of the same cell line differed profoundly in their capacity to upregulate CCL22 and IFN- β in response to dsDNA, despite apparent STING activation in both cell lines. This finding suggests that during tumor evolution, cells can acquire, or lose, the ability to upregulate CCL22. This study adds to our understanding of factors that may modulate immune activation in response to cytosolic DNA and has implications for immunotherapy strategies that activate DNA sensing pathways in cancer cells.

Introduction

Intersections between cytosolic dsDNA detection pathways and immune regulation are highly relevant to cancer immunotherapy. DNA in healthy eukaryotic cells is restricted to membraned organelles such as the nucleus and mitochondria, and its presence in the cytosol typically indicates disease or invasion by pathogens such as virus or bacteria. In cancer, cytosolic self-DNA can accumulate due to chromosomal instability, damaged mitochondria, or reactivated transposable elements such as LINE-1 (1–5). Different immunotherapy strategies also trigger cytosolic DNA sensing pathways by introducing foreign DNA into cells in the form of oncolytic viruses or plasmid DNA vaccines, or by directly activating DNA sensing pathways with pharmacological agonists.

A variety of cytoplasmic sensors, upon detection of DNA, transmit their signals to the adaptor protein STimulator of INterferon Genes (STING), which subsequently activates the transcription factors nuclear factor kappa B (NF- κ B) and interferon regulatory factor 3 (IRF3), leading to expression of type I interferons (6, 7). One of the most well-described cytosolic nucleic acid sensors upstream of STING is

cyclic GMP-AMP synthase (cGAS) (6, 7). In addition to detecting cytosolic dsDNA, cGAS reportedly responds to LINE-1 cDNA and also binds cytosolic RNA:DNA hybrids (1–5). Upon binding nucleic acid, cGAS synthesizes the second messenger cyclic dinucleotide 2'3'-cGAMP, which in turn binds STING, resulting in a conformational change and STING oligomerization. The activation cascade leads to phosphorylation of STING on serine 366 by TANK-binding kinase 1 (TBK1) and reciprocal trans-phosphorylation between TBK1 dimers (8–10). This interaction between STING and TBK1 promotes IRF3 phosphorylation and activation, resulting in IRF3 translocation to the nucleus and expression of type I interferons (8–10). NF- κ B activation in the context of the cGAS-STING pathway also depends on TBK1 and/or its homolog IKK ϵ (11–16).

STING activation promotes expression of type I interferons, leading to robust anti-viral immune responses. In the context of immunotherapy, anti-viral responses following injection of oncolytic viruses leads to rapid recruitment of Tregs via poorly understood mechanisms, which may represent a double-edged sword, as Tregs contribute to reduced viral elimination but also to decreased anti-tumor immune responses (17). In addition, STING agonists have gained widespread interest for their potential to intensify responses to established immunotherapy treatments (18, 19). However, STING activation is also reported to paradoxically contribute to pro-tumor, immunosuppressive environments (5, 20–27). Several mechanisms have been reported for the pro-tumor effects of STING, including chronic DMBA exposure (24), recruitment of myeloid-derived suppressor cells following radiation (25), and upregulation of indoleamine 2,3-dioxygenase (IDO) (20). Increased IDO can lead to elevated levels of immune checkpoint inhibitors as well as activation of regulatory T cells (Tregs) (28–30). Infiltration of Tregs into the tumor microenvironment is considered a major obstacle to successful immunotherapy due to their inhibitory effects on anti-tumor cytotoxic T cells.

A principal mechanism of Treg recruitment to the tumor microenvironment is the chemokine CCL22, also known as macrophage-derived chemokine (MDC), which binds the CCR4 receptor expressed preferentially on T cell subsets including type 2 helper T cells and Tregs (31–35). Increased CCL22 in cancer is associated with Treg recruitment and indicators of poor prognoses in multiple studies (32, 36–84). Importantly, production of CCL22 directly from malignant cells has been shown to recruit Tregs both *in vitro* and *in vivo* (37), and knockdown of CCL22 in malignant cells injected into mice decreased Foxp3 mRNA in tumors (85). These studies confirm that CCL22 expressed directly from malignant cells can recruit and retain Tregs in the tumor microenvironment. Therefore, a better understanding of factors that increase CCL22 production in malignant cells is warranted.

Previously, a link between CCL22, IDO upregulation, STING, and Treg recruitment was reported in head and neck squamous carcinoma cells (27). That study reported that c-Jun mediated CCL22 mRNA upregulation in the cell line HSC-3 by approximately 8 fold in response to cGAMP, which also increased IFN- β approximately 12 fold. Interestingly, the authors also reported that the synthetic B-DNA analog poly(dA:dT) increased IFN- β by 500 fold in a STING-independent manner yet had no greater effect on CCL22 than cGAMP. These findings raised the question of the role of the STING-IRF3-IFN- β axis in CCL22 upregulation.

The potential for STING-IRF3-IFN- β signaling to trigger CCL22 expression in malignant cells is of particular interest for immunotherapies that introduce dsDNA into cells, including DNA cancer vaccines (86–88) and oncolytic viruses (17, 89), as well as for cancer cells characterized by cytosolic self-DNA and reactivated LINE-1 retrotransposons. While investigating the effects of LINE-1 in cancer cells, we found that normal phosphodiester dsDNA containing all four nitrogenous bases could induce CCL22 mRNA by over 1,000 fold, but that the effect was cell-type dependent. The difference in magnitude between our results and the previous report utilizing poly(dA:dT) and cGAMP led us to consider whether normal B-DNA might activate CCL22 via distinct mechanisms or additional nucleic acid sensing pathways besides STING, such as toll like receptor 9 (TLR9), absent in melanoma 2 (AIM2), or DEAH box proteins. Importantly, given the critical role of IRF3-induced IFN- β for immunotherapy, we wished to clarify whether STING-mediated CCL22 upregulation occurred independently of IRF3, which might have been expected given previous reports that NF- κ B regulates CCL22 (54, 85, 90–95) and the numerous studies describing pro-tumor functions of NF- κ B, including recruitment of Tregs (96, 97). Our analysis however showed that, in the context of cytosolic dsDNA, CCL22 was regulated primarily by IRF3. We further determined that CCL22 upregulation occurred concomitantly with IFN- β activation, while previous reports have shown that IFN- α inhibited CCL22 expression (36, 98). Using CRISPR-Cas9 to knock out STING, we also determined that CCL22 upregulation by normal phosphodiester B-DNA was entirely dependent on STING, indicating that STING-independent DNA sensing pathways were not involved. Finally, we observed that two different strains of the same cell line exhibited extreme dichotomy in their upregulation of CCL22 in response to dsDNA, despite intact STING activation in both strains, suggesting that CCL22 upregulation by dsDNA can evolve in tumor cells over time. These findings add to our understanding of factors that may modulate nucleic-acid immune signaling in cancer.

Results

The chemokine CCL22 is strongly induced in tumor cells by cytoplasmic dsDNA

Figure 1A shows that HeLa cells challenged with dsDNA upregulated expression of CCL22 by over 1,000 fold, while a mock control (transfection reagent alone) had no effect. Although cytosolic dsDNA is known to elicit robust immune signaling, the effect on CCL22 was so large that we first considered potential endotoxin contamination of dsDNA, notwithstanding the use of endotoxin-free DNA purification procedures. However, treatment with DNA alone without transfection-mediated entry into cells had no effect on CCL22 (Fig. 1B).

We next sought to determine whether CpG motifs in our DNA might be responsible for CCL22 upregulation. Previous studies investigating the effect of CpG oligonucleotides on CCL22, taken together, suggest that CpGs can both inhibit and promote CCL22 expression, perhaps in a cell-type and species-specific manner (36, 65). In theory, cytosolic dsDNA containing unmethylated CpGs could be digested intracellularly to produce single-stranded CpG-containing DNA (99, 100), a potent ligand of endosomal

TLR9. To test whether CpG-mediated activation of TLR9 accounted for the upregulation of CCL22, we utilized DNA lacking linear CpG motifs to challenge cells. Figure 1A shows that CpG-free dsDNA was only slightly less efficient at upregulating CCL22, indicating that a sensor besides TLR9 was the primary driver of CCL22 expression in our system. We also confirmed that increased CCL22 mRNA resulted in increased CCL22 protein and that CCL22 was secreted into the media upon treatment of cells with dsDNA (Fig. 1C).

To determine whether dsDNA would increase CCL22 expression in other human epithelial cancer cells, five additional cell lines were tested. Two of the five cell lines were not amenable to transfection, and of the remaining three, MCF7 and HCT 116 cells upregulated CCL22 in response to dsDNA to statistically significant levels (Fig. 1D-E). Only JEG-3 cells failed to reproducibly induce CCL22 following treatment with dsDNA (Fig. 1F). These findings suggest that cytosolic dsDNA may be a common activator of CCL22 expression across different types of epithelial cancer cells. To confirm that DNA was effectively delivered to each cell line, parallel experiments were performed using a GFP expression plasmid, and GFP was subsequently visualized in live cells (Fig. 1G).

STING is essential for CCL22 upregulation in response to dsDNA

To investigate whether dsDNA activated STING in our cells, we probed for phosphorylated STING S366, which is induced by TBK1 upon cGAS detection of dsDNA (8–10). Figure 2A shows that dsDNA, with or without CpGs, increased phosphorylation of STING S366 compared to untreated cells or cells treated with a mock control (transfection reagent without DNA) or DNA alone (DNA without transfection reagent). To confirm that direct STING activation also upregulated CCL22, cells were treated with a stabilized analog of the canonical STING agonist 2'3'-cGAMP, 2'3'-cGAM(PS)2(Rp/Sp). STING activation with 2'3'-cGAM(PS)2(Rp/Sp) increased CCL22 expression in both HeLa and MCF7 cells (Fig. 2B-2C), but at lower levels than observed when treating cells with dsDNA (as shown in Fig. 1A, 1D). We did not test 2'3'-cGAM(PS)2(Rp/Sp) in HCT 116 cells due to the lower levels of dsDNA-induced CCL22 expression in these cells. Figure 2D shows that STING phosphorylation decreased to almost resting levels 24 hours after treatment with 2'3'-cGAM(PS)2(Rp/Sp), whereas treatment with dsDNA resulted in a stronger signal even after 48 hours (as shown in Fig. 2A). Thus, the lower level of CCL22 in response to 2'3'-cGAM(PS)2(Rp/Sp) might be due in part to the return of STING phosphorylation to baseline more quickly after treatment with 2'3'-cGAM(PS)2(Rp/Sp) compared to dsDNA. It may also be possible that additional dsDNA sensors that activate STING besides cGAS may lead to a stronger response compared to activation by cGAMP alone.

To determine whether STING-independent DNA sensing pathways contributed to CCL22 upregulation by dsDNA, we knocked out the STING gene (*TMEM173*) in HeLa cells using CRISPR-Cas9. To confirm that phenotypic, functional changes induced by STING knockout were specific to elimination of STING and not the result of potential off-target effects, two separate monoclonal knockout cell lines were generated, each by deleting a different region of *TMEM173* sufficient to affect all known STING splice variants. The two regions targeted for deletion are depicted in Fig. 2E. We screened monoclonal populations from

single cell limiting dilutions to identify clones carrying complete allelic deletions of the targeted region. The KO-1 and KO-2 clones selected for downstream experiments were thus confirmed for *TMEM173* deletions (Fig. 2F) and the absence of STING protein (Fig. 2G). Challenging each cell line with dsDNA revealed that STING knockout completely eliminated dsDNA-mediated upregulation of CCL22 (Fig. 2H). Parallel experiments confirmed that cells lacking STING remained capable of DNA uptake (Fig. 2I). These results confirmed that intact STING was required for dsDNA-mediated upregulation of CCL22, and that STING-independent pathways in these cells did not contribute to CCL22 expression. We next sought to determine the individual contribution of the bifurcating pathways downstream of STING on CCL22 upregulation.

Inhibition of TBK1/IKK ϵ abrogates dsDNA-mediated activation of CCL22

MRT67307 is a reversible water-soluble inhibitor of TBK1/IKK ϵ reported by the supplier (Invivogen) to specifically inhibit IRF3 with no effect on NF- κ B. Pretreatment of cells with MRT67307 led to a substantial dose-dependent decrease in dsDNA-mediated CCL22 upregulation in both HeLa and MCF7 cells (Fig. 3A-B) without affecting transfection efficiency in either cell line (Fig. 3C-D). MRT67307 also inhibited CCL22 upregulation in response to 2'3'-cGAM(PS)2(Rp/Sp) in both HeLa and MCF7 cells (Fig. 3E-F). These data suggested a role for IRF3 in dsDNA-mediated upregulation of CCL22. However, the reported IRF3-specific effect of MRT67307 was based in part on testing by the supplier that relied on activating NF- κ B with RNA hairpins, ligands for the retinoic acid-inducible gene I (RIG-1), which activates NF- κ B via IKK α /IKK β , presumably avoiding dependence on TBK1/IKK ϵ . In the context of STING-mediated activation of NF- κ B, however, several studies have reported the involvement of TBK1 and/or IKK ϵ (11–14), and TBK1/IKK ϵ has also been implicated in the phosphorylation and activation of the NF- κ B subunit RELA/p65 (15, 16). We therefore tested the effect of MRT67307 on NF- κ B activation in both STING-independent and STING-dependent conditions. MRT67307 had no observable effect on RELA/p65 phosphorylation in response to the well-known NF- κ B activators tumor necrosis factor alpha (TNF α) and phorbol 12-myristate 13-acetate (PMA) (Fig. S1A), although interestingly, PMA is also reported to activate NF- κ B in a manner dependent on IKK ϵ (101). However, MRT67307 reduced phosphorylation of RELA/p65 in response to 2'3'-cGAM(PS)2(Rp/Sp) and slightly reduced phosphorylation in response to dsDNA (Fig. S1B). These results are consistent with a previous study showing that MRT67307 slightly reduced p65 phosphorylation in response to the STING agonist DMXAA (13). We confirmed that MRT67307, as expected, inhibited phosphorylation of IRF3 (S386) in response to both 2'3'-cGAM(PS)2(Rp/Sp) and dsDNA (Fig. S1C). Since MRT67307 had an effect on phosphorylation of both IRF3 and p65 in response to dsDNA, we proceeded to use lentiviral shRNA to more specifically delineate the relative contribution of each downstream STING pathway to dsDNA-mediated upregulation of CCL22. It should also be noted that although other cGAS-STING pathway inhibitors are commercially available, many are DMSO-soluble, and we found that DMSO begins to inhibit CCL22 expression in response to dsDNA in a dose-dependent manner beginning at 0.04% (Fig. S1D).

NF- κ B contributes to CCL22 upregulation by dsDNA

Previous studies investigating the regulation of CCL22 have identified a role for NF- κ B (54, 85, 90–95). We therefore first sought to determine whether direct activation of NF- κ B with TNF α or PMA would upregulate CCL22 independent of dsDNA. Although both TNF α (Fig. 4A) and PMA (Fig. 4B) increased expression of CCL22, neither induced CCL22 to levels observed when using dsDNA (as shown in Fig. 1A). Since the functional outcome of NF- κ B depends on its mode of activation, we sought to examine the specific role of NF- κ B in the context of STING activation using RNA interference. Initially, five cell lines were created with lentiviral transduction of five different shRNA constructs from the Sigma MISSION collection and selection with puromycin. Two cell lines, one carrying shRNA p65-1 and the other p65-2, effectively knocked down RELA/p65 at the transcript (Fig. 4C) and protein levels (Fig. 4D). Stable knockdown of p65 by shRNA p65-1, but not p65-2, reduced dsDNA-mediated CCL22 upregulation to statistically significant levels (Fig. 4E), although the effect was minimal. The difference in significance between p65-1 and p65-2 shRNAs on CCL22 in Fig. 4E is consistent with the stronger knockdown mediated by p65-1 (Fig. 4C-D). Parallel transfections with a GFP expression plasmid showed intact DNA delivery to the shRNA cell lines (Fig. 4F).

IRF3 is indispensable for CCL22 upregulation by dsDNA

The relatively weak effect of NF- κ B knockdown on CCL22 upregulation compared to treatment with MRT67307, which also inhibits IRF3, suggested a predominant role for IRF3 in dsDNA-mediated upregulation of CCL22. To determine the specific contribution of IRF3, we again created two stable cell lines, each carrying one of two targeting shRNAs against IRF3 selected from a pool of five from the MISSION library that effectively knocked down IRF3 at both the transcript (Fig. 5A) and protein levels (Fig. 5B). Consistent with results using MRT67307, shRNA knockdown of IRF3 almost completely abrogated CCL22 expression in response to dsDNA, reducing the mean fold change from 1,738 (NT) to 15.7 (IRF3-1 shRNA) and 32.6 (IRF3-2 shRNA) (Fig. 5C). Parallel transfection efficiency experiments using a GFP expression plasmid confirmed that differences were not due to variation in DNA delivery between the knock down lines (Fig. 5D).

Given the effect of IRF3 knockdown on dsDNA-mediated upregulation of CCL22, a constitutively active IRF3 might be expected to further amplify CCL22 expression above levels induced by the empty plasmid. The constitutively active IRF3-5D phosphomimetic has been well-characterized in the literature and carries five aspartic acid substitutions: S396D, S398D, S402D, T404D, and S405D (102–105). As expected, IRF3-5D significantly increased CCL22 in both HeLa (Fig. 5E) and MCF7 cells (Fig. 5F) above levels observed from the empty plasmid alone.

Different strains of the same cell line differentially upregulate CCL22

Due to the large effect of dsDNA on CCL22 expression in HeLa cells, we purchased new HeLa cells from the American Type Culture Collection (ATCC) to determine whether the same effect would be observed in those cells. Remarkably, CCL-2 HeLa cells from ATCC exhibited no significant increase of CCL22 expression in response to dsDNA (Fig. 6A). To confirm the authenticity of our original HeLa cells, both

lines were sent to ATCC for short tandem repeat (STR) analysis, which showed a 100% match (Fig. 6B). We also confirmed that CCL-2 HeLa cells from ATCC were efficient at taking up dsDNA, as evidenced by GFP expression (Fig. 6C). To determine whether CCL-2 HeLa cells from ATCC were able to activate STING in response to dsDNA, STING S366 phosphorylation was compared in both cell lines. Although STING phosphorylation was reduced in CCL-2 HeLa cells from ATCC compared to our original line, it was nonetheless detectable (Fig. 6D).

dsDNA upregulates CCL22 in MCF7 cells in the absence of STING S366 phosphorylation

The lack of CCL22 upregulation in CCL-2 HeLa cells from ATCC, despite low but detectable STING phosphorylation, raised the question of whether STING S366 phosphorylation correlated with increased CCL22 in response to dsDNA in the other tested cell lines. Figure 6E shows that neither JEG-3 nor HCT 116 cells had detectable levels of STING phosphorylation following treatment with dsDNA. More surprising was the lack of observable STING S366 phosphorylation in MCF7 cells (Fig. 6E), despite its reported requirement for STING-mediated IRF3 activation by TBK1 (8–10). We confirmed IRF3 phosphorylation in MCF7 cells in response to dsDNA and also observed an increase in overall IRF3 expression (Fig. S1E). Moreover, IFN- β , which is activated by phosphorylated IRF3, was robustly upregulated in MCF7 cells by approximately 1000-fold (Fig. 6F). Interestingly, the level of dsDNA-mediated upregulation of IFN- β in HeLa cells was an order of magnitude lower (Fig. 6G) compared with MCF7 cells, despite higher levels of CCL22 in HeLa cells. Also, although CCL-2 HeLa cells from ATCC showed detectable levels of STING phosphorylation (as shown in Fig. 6D), no increase in IFN- β was detected (Fig. 6G).

Discussion

The role of cytosolic nucleic acid sensing in immune regulation is highly complex, involving multiple sensors, effector pathways, and downstream modulators. We have shown here that cytosolic dsDNA introduced into malignant cells can upregulate expression of the chemokine CCL22. CCL22 binds the CCR4 receptor on Tregs and recruits Tregs to the tumor microenvironment (31–35). Importantly, CCL22 secreted directly from malignant cells has been shown to promote Treg recruitment (37), and reducing CCL22 production in malignant cells decreased Foxp3 mRNA in tumors in mice (85). Our finding that cytosolic dsDNA can robustly upregulate CCL22 in some cancers but not others may have clinical implications for treatments with oncolytic viruses, STING agonists, or plasmid DNA tumor vaccines.

Of special interest was our finding that dsDNA upregulated CCL22 predominantly through IRF3, while NF- κ B had a more minimal role. NF- κ B, not IRF3, is well-characterized to have multiple pro-tumor effects (96, 97) and to regulate CCL22 expression in other contexts (54, 85, 90–95). However, recent studies have also begun to evaluate potential adverse effects of IRF3 on cancer outcomes (106–108). In our study, the malignant cell lines that increased CCL22 the most, HeLa and MCF7, appeared to have intact IRF3 and IFN- β activation, suggesting that this axis may be critical for CCL22 upregulation in some cancer cells.

However, a limitation to the current study is the size of the dataset tested. A much larger sampling of human cancer cells will be needed to determine the prevalence of dsDNA-mediated activation of CCL22 in malignant cells, as well as to determine whether IRF3 is a widespread mechanism. Notably, IRF3 activation triggers expression of type I interferons, yet two prior studies have reported that type I interferons inhibit CCL22/MDC (36, 98).

Our finding that dsDNA treatment of MCF7 cells resulted in IRF3 phosphorylation and concomitant activation of both IFN- β and CCL22, despite a lack of detectable phosphorylation on STING S366, remains to be explained. Apropos to this question is that, although a majority of studies report a requirement for S366 phosphorylation in STING-mediated activation of IRF3, one study reported that S366 phosphorylation can prevent the interaction between IRF3 and STING required for IRF3 phosphorylation (109, 110). While we cannot exclude the possibility that a STING-independent pathway activated IRF3 in MCF7 cells, we concluded that, in the cell line used for pathway analysis, STING was required for CCL22 upregulation.

The profound differences in CCL22 upregulation observed between the two strains of HeLa cells indicate that cancer cells can gain, or lose, the capacity to upregulate CCL22 in response to dsDNA. Cancer cell lines, particularly HeLa cells, have been well-documented to evolve in culture in response to myriad selection pressures that vary between laboratories (111). Notably, contradictory reports regarding the ability of HeLa cells to induce interferons have been reported as early as 1961 (112–114). It is unknown whether the differences observed in this study arose from a single, large-effect mutation or multiple smaller-effect mutations that collectively produced the phenotypic change, but such evolution and clonal expansion *in vivo* could conceivably contribute to acquired immune evasion.

Previous studies investigating CCL22 regulation indicate specificity based on species and cell type. For example, cell-type specific regulation of CCL22 in humans can be seen in the effects of interferon-gamma (IFN- γ), with studies reporting that IFN- γ increased CCL22 in keratinocytes (115–117), had no effect in fibroblasts (118) or airway smooth muscle cells (119), inhibited CCL22 in monocytes and macrophages (120), and was inversely correlated with CCL22 production in T cells (121). Interestingly, another nucleic acid sensing pathway, toll-like receptor 9 (TLR9), has also been implicated in CCL22 regulation, again in an apparently context-dependent manner. Unlike the cGAS-STING pathway, which detects cytosolic dsDNA, TLR9 detects single-stranded, CpG-containing DNA in endosomal compartments of sentinel immune cells. Previous reports show that the single-stranded TLR9 ligands, CpG-oligodeoxynucleotides (CpG-ODN), strongly enhanced CCL22 expression in murine dendritic cells (65), but another study concluded that CpG-ODN inhibited CCL22 in *tumor-associated* murine dendritic cells (36). Moreover, a potential species-specific regulation has also been suggested by studies showing that CpG-ODN repressed CCL22 across a range of murine bulk tumor samples (36) and in a murine asthma model (122) but increased CCL22 in cell isolates from human ovarian tumors (36). Taken together, these studies clearly show that our understanding of the variables influencing CCL22 regulation remains incomplete, and this is especially true with respect to human cancers and nucleic acid sensing. Indeed, CCL22

expression was previously thought to be absent in malignant cells, but several studies including our own have shown that CCL22 can be expressed in these cells (39, 54, 84, 85, 123–126).

Multiple studies have reported deleterious effects of elevated CCL22 in cancer (32, 36–84). A recent study also showed that in cervical cancer, intrinsic STING signaling in T cells promoted induction of Tregs (iTregs) (127). Such a scenario combined with release of CCL22 from malignant cells could conceivably retain Tregs in the tumor microenvironment, contributing to immune evasion. However, it should also be pointed out that CCL22 upregulation may not be detrimental in all cancers. Indeed, some studies have shown a protective role for CCL22, most notably in colon cancers and head and neck squamous cell carcinomas (HNSCC) (128–144). In HNSCC, studies have been divided about whether CCL22 correlates with reduced survival and metastasis (81–84) or increased survival (136–138). Although reasons for these conflicting reports remain unknown, it is interesting to note that the effect of CCL22 in HNSCC in Kaplan Meier survival analyses appears to vary with sex (e.g. Fig. S1F). It may also be possible that CCL22 and Tregs confer a protective effect in cancers in which onset and progression are associated with inflammation, such as colorectal.

Efforts to inhibit CCL22-mediated Treg recruitment in cancer have prompted recent clinical trials of the anti-CCR4 antibody mogamulizumab in advanced solid tumors, but with mixed results (32, 145–148). CCL22 recruits Tregs by binding to the receptor CCR4, and mogamulizumab has been used successfully to deplete Tregs in refractory adult T cell leukemia/lymphoma and cutaneous T cell lymphoma (31, 149, 150). Several preclinical studies showed that blocking the CCL22-CCR4 interaction also reduced Tregs in other cancers (37, 38, 151). However, a potential drawback noted for a total CCR4 blockade by agents such as mogamulizumab is that the chemokine CCL17 also binds CCR4, and CCL17 is reported to have nonredundant and even opposing functions to CCL22 (32), with CCL17 tending to promote inflammatory responses while CCL22 induces immune tolerance (65, 152). It has also been reported that an anti-CCL17 antibody failed to block Treg migration to tumors, while an anti-CCL22 antibody in the same study successfully blocked migration (38). Thus, specific antagonism of CCL22 rather than CCR4 has been suggested as a superior strategy (124). Another option would be to inhibit expression of CCL22, but this approach requires more knowledge of CCL22 regulation in cancer cells. The findings presented here offer a foundation for future studies investigating the molecular pathways regulating CCL22 in response to dsDNA in human cancer cells.

Materials And Methods

Cell culture and reagents

Cells were maintained in DMEM high glucose with GlutaMAX and pyruvate (Gibco, cat. 10569010) with 10% FBS and 1x antibiotic-antimycotic (100 units/mL penicillin, 100 ug/mL streptomycin, 0.25 ug/mL Amphotericin B; Gibco, cat. 15240096) in a humidified incubator at 37°C and 5% CO₂. Two strains of HeLa cervical adenocarcinoma cells were used: one line was a kind gift from Dr. Anthony Furano at the National Institute of Diabetes and Digestive and Kidney Diseases, originally gifted from the late Dr. Haig

Kazazian and known in the LINE-1 field as HeLa-JMV; the other strain was purchased from ATCC and designated herein as “CCL-2 HeLa ATCC”. Additional human epithelial cancer cell lines purchased from ATCC include MCF7 (mammary gland adenocarcinoma), JEG-3 (placental choriocarcinoma), and HCT 116 (colorectal carcinoma). THP-1 human leukemia monocytes were also purchased from ATCC. The STING agonist 2’3’-cGAM(PS)2(Rp/Sp) (Invivogen, cat. tlr1-nacga2srs) and IRF3 inhibitor MRT67307 (Invivogen, cat. inh-mrt) were each diluted with the companion vial of sterile, endotoxin-free LAL water and used at concentrations indicated in figure legends. STING agonists, immunostimulatory dsDNA (pcDNA3.1(+)-puro) and CpG-free dsDNA (pCpGfree-mcs, Invivogen) were transfected using Opti-MEM (Gibco, cat. 31-985-062) as the DNA diluent and either TransIT-LT1 (Mirus, cat. MIR 2300), TransfeX (ATCC, cat. ACS-4005), or TransIT-X2 (Mirus, cat. MIR 6000) based on transfection optimization experiments for each cell line, with the reagent and ratios indicated in figure legends. All cell lines were monitored for mycoplasma using the LookOut mycoplasma PCR detection kit (Sigma-Aldrich, cat. MP0035). THP-1 positive controls for phospho-STING (S366) were generated by plating THP-1 cells in RPMI 1640 media supplemented with 10% FBS and 80 nM PMA for 48 hours to promote differentiation to macrophages before transfecting with pcDNA3.1 (3 µg/mL) using Lipofectamine 3000 at a 1:1 ratio; cells were harvested 4 hours post transfection in 3% SDS, 25 mM Tris-HCl pH 7.4, and 0.5 mM EDTA supplemented with HALT protease and phosphatase inhibitor cocktail at 3X (ThermoFisher, cat. 78440).

Plasmids and cloning

pcDNA3.1(+)-neo was obtained from ThermoFisher (Invitrogen cat. V790-20). pcDNA3.1(+)-neo-IRF3-5D was created using the wild-type template Human V5-IRF3-pcDNA3, a gift from Saumen Sarkar (Addgene plasmid # 32713; <http://n2t.net/addgene:32713>; RRID:Addgene_32713, (153)) and the Q5 site-directed mutagenesis kit (NEB, cat. E0554S) with the forward and reverse primers 5’-CTCGATCTCGACGATGACCAGTACAAGGCCTAC and 5’-TGGGTGGTTCGTTGTCAATGTGCAGGTCCACAGT respectively; mutations were confirmed with sequencing. pCpGf-Bsr-GFP was constructed by PCR-amplifying GFP obtained from pSELECT-zeo-GFPBsr (Invivogen, cat. psetz-zgfpbsr) with a Kozak sequence encoded on the forward primer, then inserting it into pCpGfree-vitroBmcs (Invivogen, cat. pcpgvb-mcsg2) digested with BglII and ApaI; insertion was confirmed with sequencing. pcDNA3.1(+)-puro was previously described (154). pCpGfree-mcs was obtained from Invivogen (cat. pcpgf-mcs). pX333, carrying two tandem U6 promoters that simultaneously drive expression of two independent guide RNAs (gRNAs) in addition to the Cas9 nuclease, was a gift from Andrea Ventura (Addgene plasmid # 64073; <http://n2t.net/addgene:64073> ; RRID:Addgene_64073) (155). pX333-TMEM173-KO-1, carrying gRNA-1 and gRNA-2, was generated by first digesting pX333 with BsaI and inserting annealed oligos encoding the first gRNA (gRNA-1) with 5’ and 3’ overhangs complementary to the cohesive ends resulting from BsaI digestion. Next, the plasmid containing gRNA-1 was digested with BbsI to insert annealed oligos encoding the second gRNA (gRNA-2), also with 5’ and 3’ overhangs complementary to ends resulting from BbsI digestion (note that BbsI and BsaI have distinct recognition sequences but the same cohesive end sequences). Oligos used to make pX333-TMEM173-KO-1, with overhangs noted in lower case, are 5’-caccGGCCTCAAGGTATGACACAG and 5’-aaacCTGTGTCATACCTTGAGGCC (gRNA-1) and 5’-caccGGCTGTCACTCACAGGTACC and 5’-

aaacGGTACCTGTGAGTGACAGCC (gRNA-2). pX333-TMEM173-KO-2, containing sequences for gRNA-3 and gRNA-4, was generated as described above, with oligo sequences 5'-caccGGGAATTTCAACGTGGCCCA and 5'-aaacTGGGCCACGTTGAAATTC (gRNA-3) and 5'-caccGAAGGGCGGGCCGACCGCATT and 5'-aaacAATGCGGTGCGCCCGCCCTTC (gRNA-4). Screening to confirm insertion of gRNAs into pX333 was performed using either diagnostic digestion incorporating AflIII (NEB, cat. R0520S), which is destroyed upon insertion of gRNA into the BsaI site (assuming the gRNA does not harbor an AflIII site), or colony PCR with primers specific for the gRNA(s); final clones were verified with sequencing. Lentiviral plasmids included the packaging plasmid psPAX2 (Addgene plasmid # 12260; <http://n2t.net/addgene:12260>; RRID:Addgene_12260) and the envelope plasmid pMD2.G (Addgene plasmid # 12259; <http://n2t.net/addgene:12259>; RRID:Addgene_12259), both gifts from Didier Trono. All RNAi lentiviral expression vectors were constructed using pLKO.1-puro, version 1, from The RNAi Consortium (TRC) library collection. RNAi sequences included control shRNA (Sigma-Aldrich, cat. SHC002), RELA/p65 shRNA-1 (Sigma-Aldrich, cat. TRCN0000014687), RELA/p65 shRNA-2 (Sigma-Aldrich, cat. TRCN0000014684), IRF3 shRNA-1 (Sigma-Aldrich, cat. TRCN0000005921), and IRF3 shRNA-2 (Sigma-Aldrich, cat. TRCN0000005923). All ss oligos were purchased from IDT. DNA for experiments was obtained using endotoxin-free plasmid purification kits (NucleoBond Xtra Midi EF, Takara, cat. 740420.10 or Qiagen EndoFree Plasmid Maxi Kit, cat. 12362); concentration and purity were assessed with spectrophotometry and agarose electrophoresis.

CRISPR-Cas9 gRNA design

Sequences for gRNAs targeting *TMEM173*, which encodes the protein STING, were designed and analyzed using multiple in-silico softwares, including Synthego V1.3 (<https://design.synthego.com/#/>), ATUM gRNA Design Tool (<https://www.atum.bio/eCommerce/cas9/input>), Cas-Designer (<http://www.rgenome.net/cas-designer/>) (156), and Cas-OFFinder (<http://www.rgenome.net/cas-offinder/>) (157). To confirm the absence of polymorphisms that might affect gRNA binding in HeLa cells, gRNA sequences were checked against the sequence of *TMEM173* amplified from HeLa cell genomic DNA with the forward primer (TMEM-F) 5'-CACTCCAGGTGACTCACTGCAGTAC and reverse primer (TMEM-R) 5'-CCTTTCTGCAAAGTAGGCATCATAGCAA.

Generation of CRISPR-Cas9 edited monoclonal cell lines

HeLa cells were seeded at 3.7×10^5 cells per well in a 6-well plate or 1.5×10^5 cells per well in a 12-well plate. The plasmids pX333-TMEM173-KO-1 or -KO-2 were transfected at a final DNA concentration of 1.61 $\mu\text{g}/\text{mL}$ using TransIT-LT1 transfection reagent. Medium was changed approximately 24 hours post transfection. The following day, limiting dilution was performed to isolate single cells in 96-well plates. Overall knockout efficiency was estimated by comparing relative band intensities of PCR amplicons derived from deleted and unedited genomic DNA harvested from heterogeneous knockout cell populations 48 hours after transfection with pX333 and amplified with the primers TMEM-F and TMEM-R. Monoclonal populations were subsequently screened as just described, and clones exhibiting complete allelic knock out were analyzed for STING protein expression with Western blots. Knockout cell lines were maintained in DMEM high glucose with GlutaMAX and pyruvate with 10% FBS and 1x antibiotic-antimycotic.

Lentiviral transductions and establishment of stable cell lines

HEK293 cells were seeded at 9×10^5 cells per well in 6-well plates and transfected 24 hours later with 1 μ g total DNA containing psPAX2, pMD2.G, and each pLKO.1-puro RNAi expression plasmid at a 1:0.25:0.75 ratio, respectively, with TransIT-X2 used at a 1:2 ratio of μ g DNA to μ L X2. HeLa cells were plated 24 hours prior to transduction at 4×10^5 cells per well in 6-well plates. Media were collected from HEK293 cells 48 hours after transfection and used for transductions in a final concentration of 8 μ g/mL polybrene (Sigma-Aldrich, cat. TR-1003). Selection and maintenance of transduced cells was achieved with 5 μ g/mL puromycin (Gibco, cat. A1113803) begun 24 hours after application of lentiviral-containing media.

Live-cell imaging

Live cells were imaged for GFP expression using an EVOS FLoid imaging system. Images were processed using Image J.

Cell lysis, immunoblots, and antibodies

Cells were lysed for immunoblotting with 3% SDS, 25 mM Tris-HCl pH 7.4, and 0.5 mM EDTA supplemented with 3X HALT protease and phosphatase inhibitor cocktail (ThermoFisher, cat. 78440). Lysates were homogenized with QIAshredder columns (Qiagen, cat. 79656), and protein concentration was determined using the BioRad DC Protein Assay (cat. 5000112). Proteins were transferred onto low-fluorescent PVDF membranes (BioRad, cat. 1704274 or Millipore Immobilon-FL, cat. IPFL10100) using either a wet tank with tris-glycine buffer plus 20% (v/v) methanol or a semi-dry system (BioRad Trans-Blot Turbo Transfer System). Primary antibodies to the following human proteins were used: STING (Abcam ab181125); phospho-STING (S366, Cell Signaling Technology, cat. 19781S); RELA/p65 (R&D, cat. AF5078-SP); phospho-RELA/p65 (S536, R&D, cat. MAB72261-SP); IRF3 (R&D, cat. AF4019-SP); phospho-IRF3 (S386, Cell Signaling Technology, cat. 37829T); and beta-tubulin loading control (Abcam, cat. ab6046). Fluorescent secondary antibodies were IRDye 680RD and IRDye 800CW (Li-Cor). Blots were imaged with an infrared Li-Cor Odyssey CLx Imager and processed using Image Studio (Li-Cor).

ELISA

CCL22 protein was measured in media harvested from cells using an ELISA (Abcam, cat. ab100591) performed according to the manufacturer's instructions.

RNA purification and RTqPCR

RNA was isolated by lysing cells in TRIzol reagent (Invitrogen, cat. 15596026) followed by column purification and on-column DNase digestion according to the TRIzol two-step protocol from the Monarch total RNA miniprep kit (NEB, cat. T2010S) or PureLink RNA mini kit (Ambion, cat. 12183018A and

12185010). Quality and concentration were assessed with spectrophotometry. First-strand cDNA synthesis was performed using LunaScript RT SuperMix Kit (NEB, cat. E3010S). qPCR was performed on a QuantStudio 3 or StepOnePlus real-time PCR machine using TaqMan Fast Advanced Master Mix (Applied Biosystems, cat. A44359) and the following TaqMan Assays (assay ID in parenthesis following gene name): CCL22 (Hs00171080); RELA/p65 (Hs00153294_m1); IRF3 (Hs01547283_m1); GAPDH (Hs02786624_g1); beta actin (Hs99999903), 18s (Hs99999901); and IFN- β (Hs01077958_s1). All qPCR samples were assayed with technical triplicates. Data were analyzed using the delta-delta Ct method; housekeeping genes were averaged using the geometric mean.

Declarations

ACKNOWLEDGEMENTS

We wish to thank Dr. James Drummond and Dr. Robert McKallip for their helpful suggestions during the course of the study. We also thank Dr. James Drummond for his helpful comments to improve the manuscript. We would also like to thank Dr. Anthony Furano, Dr. John Moran, and the late Dr. Haig Kazazian for the kind gift of HeLa cells.

FUNDING

This work was supported by startup funds and a Dean's Seed Grant from Mercer University School of Medicine, Macon GA, USA.

CONFLICT OF INTEREST

The authors declare they have no competing interests.

DATA AVAILABILITY

All data were reported in the figures. Whole images of Western blots, ELISA absorbance data, and RTqPCR raw data are available upon request.

REAGENT AVAILABILITY

The HeLa cell line used in this study that was obtained from the Kazazian and Moran laboratories through Dr. Anthony Furano at NIDDK will be made available upon request. This cell line is also available from multiple laboratories that investigate LINE-1.

AUTHOR CREDITS

Jihyun Kim: conceptualization, experimentation, supervision, writing (review and editing). Jocelyn V. Pena: experimentation, supervision, writing (review and editing). Hannah P. McQueen: experimentation. Lingwei Kong: experimentation, supervision, writing (review and editing). Dina Michael: experimentation.

Pamela R. Cook: conceptualization, methodology, analysis, experimentation, supervision, writing (original draft).

References

1. Simon M, Van Meter M, Ablaeva J, Ke Z, Gonzalez RS, Taguchi T, et al. LINE1 Derepression in Aged Wild-Type and SIRT6-Deficient Mice Drives Inflammation. *Cell Metab.* 2019;29(4):871-85 e5.
2. Stetson DB, Ko JS, Heidmann T, Medzhitov R. Trex1 prevents cell-intrinsic initiation of autoimmunity. *Cell.* 2008;134(4):587-98.
3. Thomas CA, Tejwani L, Trujillo CA, Negraes PD, Herai RH, Mesci P, et al. Modeling of TREX1-Dependent Autoimmune Disease using Human Stem Cells Highlights L1 Accumulation as a Source of Neuroinflammation. *Cell Stem Cell.* 2017;21(3):319-31 e8.
4. De Cecco M, Ito T, Petrashen AP, Elias AE, Skvir NJ, Criscione SW, et al. Author Correction: L1 drives IFN in senescent cells and promotes age-associated inflammation. *Nature.* 2019;572(7767):E5.
5. Decout A, Katz JD, Venkatraman S, Ablasser A. The cGAS-STING pathway as a therapeutic target in inflammatory diseases. *Nat Rev Immunol.* 2021;21(9):548-69.
6. Hopfner KP, Hornung V. Molecular mechanisms and cellular functions of cGAS-STING signalling. *Nat Rev Mol Cell Biol.* 2020;21(9):501-21.
7. Yu L, Liu P. Cytosolic DNA sensing by cGAS: regulation, function, and human diseases. *Signal Transduct Target Ther.* 2021;6(1):170.
8. Tanaka Y, Chen ZJ. STING specifies IRF3 phosphorylation by TBK1 in the cytosolic DNA signaling pathway. *Sci Signal.* 2012;5(214):ra20.
9. Liu S, Cai X, Wu J, Cong Q, Chen X, Li T, et al. Phosphorylation of innate immune adaptor proteins MAVS, STING, and TRIF induces IRF3 activation. *Science.* 2015;347(6227):aaa2630.
10. Zhang C, Shang G, Gui X, Zhang X, Bai XC, Chen ZJ. Structural basis of STING binding with and phosphorylation by TBK1. *Nature.* 2019;567(7748):394-8.
11. Abe T, Barber GN. Cytosolic-DNA-mediated, STING-dependent proinflammatory gene induction necessitates canonical NF-kappaB activation through TBK1. *J Virol.* 2014;88(10):5328-41.
12. Fang R, Wang C, Jiang Q, Lv M, Gao P, Yu X, et al. NEMO-IKKbeta Are Essential for IRF3 and NF-kappaB Activation in the cGAS-STING Pathway. *J Immunol.* 2017;199(9):3222-33.
13. Balka KR, Louis C, Saunders TL, Smith AM, Calleja DJ, D'Silva DB, et al. TBK1 and IKKepsilon Act Redundantly to Mediate STING-Induced NF-kappaB Responses in Myeloid Cells. *Cell Rep.* 2020;31(1):107492.
14. Yum S, Li M, Fang Y, Chen ZJ. TBK1 recruitment to STING activates both IRF3 and NF-kappaB that mediate immune defense against tumors and viral infections. *Proc Natl Acad Sci U S A.* 2021;118(14).
15. Christian F, Smith EL, Carmody RJ. The Regulation of NF-kappaB Subunits by Phosphorylation. *Cells.* 2016;5(1).

16. Mattioli I, Geng H, Sebald A, Hodel M, Bucher C, Kracht M, et al. Inducible phosphorylation of NF-kappa B p65 at serine 468 by T cell costimulation is mediated by IKK epsilon. *J Biol Chem.* 2006;281(10):6175-83.
17. Gujar S, Pol JG, Kim Y, Lee PW, Kroemer G. Antitumor Benefits of Antiviral Immunity: An Underappreciated Aspect of Oncolytic Virotherapies. *Trends Immunol.* 2018;39(3):209-21.
18. Amouzegar A, Chelvanambi M, Filderman JN, Storkus WJ, Luke JJ. STING Agonists as Cancer Therapeutics. *Cancers (Basel).* 2021;13(11).
19. Ou L, Zhang A, Cheng Y, Chen Y. The cGAS-STING Pathway: A Promising Immunotherapy Target. *Front Immunol.* 2021;12:795048.
20. Lemos H, Mohamed E, Huang L, Ou R, Pacholczyk G, Arbab AS, et al. STING Promotes the Growth of Tumors Characterized by Low Antigenicity via IDO Activation. *Cancer Res.* 2016;76(8):2076-81.
21. Kwon J, Bakhoun SF. The Cytosolic DNA-Sensing cGAS-STING Pathway in Cancer. *Cancer Discov.* 2020;10(1):26-39.
22. Jiang M, Chen P, Wang L, Li W, Chen B, Liu Y, et al. cGAS-STING, an important pathway in cancer immunotherapy. *J Hematol Oncol.* 2020;13(1):81.
23. Bakhoun SF, Ngo B, Laughney AM, Cavallo JA, Murphy CJ, Ly P, et al. Chromosomal instability drives metastasis through a cytosolic DNA response. *Nature.* 2018;553(7689):467-72.
24. Ahn J, Xia T, Konno H, Konno K, Ruiz P, Barber GN. Inflammation-driven carcinogenesis is mediated through STING. *Nat Commun.* 2014;5:5166.
25. Liang H, Deng L, Hou Y, Meng X, Huang X, Rao E, et al. Host STING-dependent MDSC mobilization drives extrinsic radiation resistance. *Nat Commun.* 2017;8(1):1736.
26. Hou Y, Liang H, Rao E, Zheng W, Huang X, Deng L, et al. Non-canonical NF-kappaB Antagonizes STING Sensor-Mediated DNA Sensing in Radiotherapy. *Immunity.* 2018;49(3):490-503 e4.
27. Liang D, Xiao-Feng H, Guan-Jun D, Er-Ling H, Sheng C, Ting-Ting W, et al. Activated STING enhances Tregs infiltration in the HPV-related carcinogenesis of tongue squamous cells via the c-jun/CCL22 signal. *Biochim Biophys Acta.* 2015;1852(11):2494-503.
28. Liu M, Wang X, Wang L, Ma X, Gong Z, Zhang S, et al. Targeting the IDO1 pathway in cancer: from bench to bedside. *J Hematol Oncol.* 2018;11(1):100.
29. Meireson A, Devos M, Brochez L. IDO Expression in Cancer: Different Compartment, Different Functionality? *Front Immunol.* 2020;11:531491.
30. Munn DH, Mellor AL. IDO in the Tumor Microenvironment: Inflammation, Counter-Regulation, and Tolerance. *Trends Immunol.* 2016;37(3):193-207.
31. Sugiyama D, Nishikawa H, Maeda Y, Nishioka M, Tanemura A, Katayama I, et al. Anti-CCR4 mAb selectively depletes effector-type FoxP3+CD4+ regulatory T cells, evoking antitumor immune responses in humans. *Proc Natl Acad Sci U S A.* 2013;110(44):17945-50.
32. Yoshie O. CCR4 as a Therapeutic Target for Cancer Immunotherapy. *Cancers (Basel).* 2021;13(21).

33. Yoshie O, Matsushima K. CCR4 and its ligands: from bench to bedside. *Int Immunol.* 2015;27(1):11-20.
34. Nishikawa H, Sakaguchi S. Regulatory T cells in tumor immunity. *Int J Cancer.* 2010;127(4):759-67.
35. Kohli K, Pillarisetty VG, Kim TS. Key chemokines direct migration of immune cells in solid tumors. *Cancer Gene Ther.* 2022;29(1):10-21.
36. Anz D, Rapp M, Eiber S, Koelzer VH, Thaler R, Haubner S, et al. Suppression of intratumoral CCL22 by type I interferon inhibits migration of regulatory T cells and blocks cancer progression. *Cancer Res.* 2015;75(21):4483-93.
37. Chang DK, Peterson E, Sun J, Goudie C, Drapkin RI, Liu JF, et al. Anti-CCR4 monoclonal antibody enhances antitumor immunity by modulating tumor-infiltrating Tregs in an ovarian cancer xenograft humanized mouse model. *Oncoimmunology.* 2016;5(3):e1090075.
38. Curiel TJ, Coukos G, Zou L, Alvarez X, Cheng P, Mottram P, et al. Specific recruitment of regulatory T cells in ovarian carcinoma fosters immune privilege and predicts reduced survival. *Nat Med.* 2004;10(9):942-9.
39. Faget J, Biota C, Bachelot T, Gobert M, Treilleux I, Goutagny N, et al. Early detection of tumor cells by innate immune cells leads to T(reg) recruitment through CCL22 production by tumor cells. *Cancer Res.* 2011;71(19):6143-52.
40. Fang QL, Li KC, Wang L, Gu XL, Song RJ, Lu S. Targeted Inhibition of CCL22 by miR-130a-5p Can Enhance the Sensitivity of Cisplatin-Resistant Gastric Cancer Cells to Chemotherapy. *Cancer Manag Res.* 2020;12:3865-75.
41. Furudate S, Fujimura T, Kambayashi Y, Kakizaki A, Hidaka T, Aiba S. Immunomodulatory Effect of Imiquimod Through CCL22 Produced by Tumor-associated Macrophages in B16F10 Melanomas. *Anticancer Res.* 2017;37(7):3461-71.
42. Gao Y, Fan X, Li N, Du C, Yang B, Qin W, et al. CCL22 signaling contributes to sorafenib resistance in hepatitis B virus-associated hepatocellular carcinoma. *Pharmacol Res.* 2020;157:104800.
43. Gobert M, Treilleux I, Bendriss-Vermare N, Bachelot T, Goddard-Leon S, Arfi V, et al. Regulatory T cells recruited through CCL22/CCR4 are selectively activated in lymphoid infiltrates surrounding primary breast tumors and lead to an adverse clinical outcome. *Cancer Res.* 2009;69(5):2000-9.
44. Ibrahim OM, Basse PH, Jiang W, Guru K, Chatta G, Kalinski P. NF-kappaB-Activated COX2/PGE2/EP4 Axis Controls the Magnitude and Selectivity of BCG-Induced Inflammation in Human Bladder Cancer Tissues. *Cancers (Basel).* 2021;13(6).
45. Jafarzadeh A, Fooladseresht H, Minaee K, Bazrafshani MR, Khosravimashizi A, Nemati M, et al. Higher circulating levels of chemokine CCL22 in patients with breast cancer: evaluation of the influences of tumor stage and chemokine gene polymorphism. *Tumour Biol.* 2015;36(2):1163-71.
46. Jiang Z, Chen H, Su M, Wu L, Yu X, Liu Z. MicroRNA-23a-3p influences the molecular mechanism of gastric cancer cells via CCL22/PI3K/Akt axis. *Bioengineered.* 2021;12(2):11277-87.
47. Jin C, Shi L, Li Z, Liu W, Zhao B, Qiu Y, et al. Circ_0039569 promotes renal cell carcinoma growth and metastasis by regulating miR-34a-5p/CCL22. *Am J Transl Res.* 2019;11(8):4935-45.

48. Jorapur A, Marshall LA, Jacobson S, Xu M, Marubayashi S, Zibinsky M, et al. EBV+ tumors exploit tumor cell-intrinsic and -extrinsic mechanisms to produce regulatory T cell-recruiting chemokines CCL17 and CCL22. *PLoS Pathog.* 2022;18(1):e1010200.
49. Klarquist J, Tobin K, Farhangi Oskuei P, Henning SW, Fernandez MF, Dellacecca ER, et al. Ccl22 Diverts T Regulatory Cells and Controls the Growth of Melanoma. *Cancer Res.* 2016;76(21):6230-40.
50. Kumai T, Nagato T, Kobayashi H, Komabayashi Y, Ueda S, Kishibe K, et al. CCL17 and CCL22/CCR4 signaling is a strong candidate for novel targeted therapy against nasal natural killer/T-cell lymphoma. *Cancer Immunol Immunother.* 2015;64(6):697-705.
51. Kumar S, Wilkes DW, Samuel N, Blanco MA, Nayak A, Alicea-Torres K, et al. DeltaNp63-driven recruitment of myeloid-derived suppressor cells promotes metastasis in triple-negative breast cancer. *J Clin Invest.* 2018;128(11):5095-109.
52. Lee HK, Ji HJ, Shin SK, Koo J, Kim TH, Kim CW, et al. Targeting transforming growth factor-beta2 by antisense oligodeoxynucleotide accelerates T cell-mediated tumor rejection in a humanized mouse model of triple-negative breast cancer. *Cancer Immunol Immunother.* 2022.
53. Li YQ, Liu FF, Zhang XM, Guo XJ, Ren MJ, Fu L. Tumor secretion of CCL22 activates intratumoral Treg infiltration and is independent prognostic predictor of breast cancer. *PLoS One.* 2013;8(10):e76379.
54. Li ZQ, Wang HY, Zeng QL, Yan JY, Hu YS, Li H, et al. p65/miR-23a/CCL22 axis regulated regulatory T cells recruitment in hepatitis B virus positive hepatocellular carcinoma. *Cancer Med.* 2020;9(2):711-23.
55. Liu N, Chang CW, Steer CJ, Wang XW, Song G. MicroRNA-15a/16-1 Prevents Hepatocellular Carcinoma by Disrupting the Communication Between Kupffer Cells and Regulatory T Cells. *Gastroenterology.* 2022;162(2):575-89.
56. Liu Y, Zhang H, Zhang W, Xiang L, Yin Z, Xu H, et al. circ_0004140 promotes LUAD tumor progression and immune resistance through circ_0004140/miR-1184/CCL22 axis. *Cell Death Discov.* 2022;8(1):181.
57. Mailloux AW, Young MR. NK-dependent increases in CCL22 secretion selectively recruits regulatory T cells to the tumor microenvironment. *J Immunol.* 2009;182(5):2753-65.
58. Maolake A, Izumi K, Shigehara K, Natsagdorj A, Iwamoto H, Kadomoto S, et al. Tumor-associated macrophages promote prostate cancer migration through activation of the CCL22-CCR4 axis. *Oncotarget.* 2017;8(6):9739-51.
59. Marshall LA, Marubayashi S, Jorapur A, Jacobson S, Zibinsky M, Robles O, et al. Tumors establish resistance to immunotherapy by regulating T(reg) recruitment via CCR4. *J Immunother Cancer.* 2020;8(2).
60. Maruyama T, Kono K, Izawa S, Mizukami Y, Kawaguchi Y, Mimura K, et al. CCL17 and CCL22 chemokines within tumor microenvironment are related to infiltration of regulatory T cells in esophageal squamous cell carcinoma. *Dis Esophagus.* 2010;23(5):422-9.

61. Mizukami Y, Kono K, Kawaguchi Y, Akaike H, Kamimura K, Sugai H, et al. CCL17 and CCL22 chemokines within tumor microenvironment are related to accumulation of Foxp3+ regulatory T cells in gastric cancer. *Int J Cancer*. 2008;122(10):2286-93.
62. Muthuswamy R, Corman JM, Dahl K, Chatta GS, Kalinski P. Functional reprogramming of human prostate cancer to promote local attraction of effector CD8(+) T cells. *Prostate*. 2016;76(12):1095-105.
63. Qi Q, Zhuang L, Shen Y, Geng Y, Yu S, Chen H, et al. A novel systemic inflammation response index (SIRI) for predicting the survival of patients with pancreatic cancer after chemotherapy. *Cancer*. 2016;122(14):2158-67.
64. Qin XJ, Shi HZ, Deng JM, Liang QL, Jiang J, Ye ZJ. CCL22 recruits CD4-positive CD25-positive regulatory T cells into malignant pleural effusion. *Clinical cancer research : an official journal of the American Association for Cancer Research*. 2009;15(7):2231-7.
65. Rapp M, Wintergerst MWM, Kunz WG, Vetter VK, Knott MML, Lisowski D, et al. CCL22 controls immunity by promoting regulatory T cell communication with dendritic cells in lymph nodes. *J Exp Med*. 2019;216(5):1170-81.
66. Sallam MA, Wyatt Shields Iv C, Prakash S, Kim J, Pan DC, Mitragotri S. A dual macrophage polarizer conjugate for synergistic melanoma therapy. *J Control Release*. 2021;335:333-44.
67. Song NY, Li X, Ma B, Willette-Brown J, Zhu F, Jiang C, et al. IKKalpha-deficient lung adenocarcinomas generate an immunosuppressive microenvironment by overproducing Treg-inducing cytokines. *Proc Natl Acad Sci U S A*. 2022;119(6).
68. Wang D, Yang L, Yue D, Cao L, Li L, Wang D, et al. Macrophage-derived CCL22 promotes an immunosuppressive tumor microenvironment via IL-8 in malignant pleural effusion. *Cancer Lett*. 2019;452:244-53.
69. Wang Q, Schmoeckel E, Kost BP, Kuhn C, Vattai A, Vilsmaier T, et al. Higher CCL22+ Cell Infiltration is Associated with Poor Prognosis in Cervical Cancer Patients. *Cancers (Basel)*. 2019;11(12).
70. Wei C, Yang C, Wang S, Shi D, Zhang C, Lin X, et al. M2 macrophages confer resistance to 5-fluorouracil in colorectal cancer through the activation of CCL22/PI3K/AKT signaling. *Onco Targets Ther*. 2019;12:3051-63.
71. Wei Y, Wang T, Song H, Tian L, Lyu G, Zhao L, et al. C-C motif chemokine 22 ligand (CCL22) concentrations in sera of gastric cancer patients are related to peritoneal metastasis and predict recurrence within one year after radical gastrectomy. *J Surg Res*. 2017;211:266-78.
72. Wiedemann GM, Knott MM, Vetter VK, Rapp M, Haubner S, Fessler J, et al. Cancer cell-derived IL-1 α induces CCL22 and the recruitment of regulatory T cells. *Oncoimmunology*. 2016;5(9):e1175794.
73. Wiedemann GM, Röhrle N, Makeschin MC, Fessler J, Endres S, Mayr D, et al. Peritumoural CCL1 and CCL22 expressing cells in hepatocellular carcinomas shape the tumour immune infiltrate. *Pathology*. 2019;51(6):586-92.
74. Wilson AL, Moffitt LR, Wilson KL, Bilandzic M, Wright MD, Gorrell MD, et al. DPP4 Inhibitor Sitagliptin Enhances Lymphocyte Recruitment and Prolongs Survival in a Syngeneic Ovarian Cancer Mouse

- Model. *Cancers (Basel)*. 2021;13(3).
75. Wolf-Dennen K, Gordon N, Kleinerman ES. Exosomal communication by metastatic osteosarcoma cells modulates alveolar macrophages to an M2 tumor-promoting phenotype and inhibits tumoricidal functions. *Oncoimmunology*. 2020;9(1):1747677.
76. Wu S, He H, Liu H, Cao Y, Li R, Zhang H, et al. C-C motif chemokine 22 predicts postoperative prognosis and adjuvant chemotherapeutic benefits in patients with stage II/III gastric cancer. *Oncoimmunology*. 2018;7(6):e1433517.
77. Yang P, Li QJ, Feng Y, Zhang Y, Markowitz GJ, Ning S, et al. TGF-beta-miR-34a-CCL22 signaling-induced Treg cell recruitment promotes venous metastases of HBV-positive hepatocellular carcinoma. *Cancer Cell*. 2012;22(3):291-303.
78. Yeung OW, Lo CM, Ling CC, Qi X, Geng W, Li CX, et al. Alternatively activated (M2) macrophages promote tumour growth and invasiveness in hepatocellular carcinoma. *J Hepatol*. 2015;62(3):607-16.
79. Zaynagetdinov R, Sherrill TP, Gleaves LA, McLoed AG, Saxon JA, Habermann AC, et al. Interleukin-5 facilitates lung metastasis by modulating the immune microenvironment. *Cancer Res*. 2015;75(8):1624-34.
80. Zhao X, Liu S, Chen X, Zhao J, Li F, Zhao Q, et al. L1CAM overexpression promotes tumor progression through recruitment of regulatory T cells in esophageal carcinoma. *Cancer Biol Med*. 2021.
81. Huang YH, Chang CY, Kuo YZ, Fang WY, Kao HY, Tsai ST, et al. Cancer-associated fibroblast-derived interleukin-1beta activates protumor C-C motif chemokine ligand 22 signaling in head and neck cancer. *Cancer Sci*. 2019;110(9):2783-93.
82. Kimura S, Nanbu U, Noguchi H, Harada Y, Kumamoto K, Sasaguri Y, et al. Macrophage CCL22 expression in the tumor microenvironment and implications for survival in patients with squamous cell carcinoma of the tongue. *J Oral Pathol Med*. 2019;48(8):677-85.
83. Kimura S, Noguchi H, Nanbu U, Nakayama T. Macrophage CCL22 expression promotes lymphangiogenesis in patients with tongue squamous cell carcinoma via IL-4/STAT6 in the tumor microenvironment. *Oncol Lett*. 2021;21(5):383.
84. Tsujikawa T, Yaguchi T, Ohmura G, Ohta S, Kobayashi A, Kawamura N, et al. Autocrine and paracrine loops between cancer cells and macrophages promote lymph node metastasis via CCR4/CCL22 in head and neck squamous cell carcinoma. *Int J Cancer*. 2013;132(12):2755-66.
85. Huang YH, Chang CY, Kuo YZ, Fang WY, Kao HY, Tsai ST, et al. Cancer-associated fibroblast-derived interleukin-1 β activates protumor C-C motif chemokine ligand 22 signaling in head and neck cancer. *Cancer Sci*. 2019;110(9):2783-93.
86. Tanaka A, Sakaguchi S. Targeting Treg cells in cancer immunotherapy. *Eur J Immunol*. 2019;49(8):1140-6.
87. Chen BJ, Zhao JW, Zhang DH, Zheng AH, Wu GQ. Immunotherapy of Cancer by Targeting Regulatory T cells. *Int Immunopharmacol*. 2022;104:108469.

88. Lopes A, Vandermeulen G, Preat V. Cancer DNA vaccines: current preclinical and clinical developments and future perspectives. *J Exp Clin Cancer Res.* 2019;38(1):146.
89. Yang L, Gu X, Yu J, Ge S, Fan X. Oncolytic Virotherapy: From Bench to Bedside. *Front Cell Dev Biol.* 2021;9:790150.
90. Poole E, Atkins E, Nakayama T, Yoshie O, Groves I, Alcami A, et al. NF-kappaB-mediated activation of the chemokine CCL22 by the product of the human cytomegalovirus gene UL144 escapes regulation by viral IE86. *J Virol.* 2008;82(9):4250-6.
91. Nakayama T, Hieshima K, Nagakubo D, Sato E, Nakayama M, Kawa K, et al. Selective induction of Th2-attracting chemokines CCL17 and CCL22 in human B cells by latent membrane protein 1 of Epstein-Barr virus. *J Virol.* 2004;78(4):1665-74.
92. Sun J, Sun J, Song B, Zhang L, Shao Q, Liu Y, et al. Fucoidan inhibits CCL22 production through NF-kappaB pathway in M2 macrophages: a potential therapeutic strategy for cancer. *Sci Rep.* 2016;6:35855.
93. Ghadially H, Ross XL, Kerst C, Dong J, Reske-Kunz AB, Ross R. Differential regulation of CCL22 gene expression in murine dendritic cells and B cells. *J Immunol.* 2005;174(9):5620-9.
94. Qi XF, Kim DH, Yoon YS, Li JH, Song SB, Jin D, et al. The adenylyl cyclase-cAMP system suppresses TARC/CCL17 and MDC/CCL22 production through p38 MAPK and NF-kappaB in HaCaT keratinocytes. *Mol Immunol.* 2009;46(10):1925-34.
95. Kwon DJ, Bae YS, Ju SM, Goh AR, Youn GS, Choi SY, et al. Casuarinin suppresses TARC/CCL17 and MDC/CCL22 production via blockade of NF-kappaB and STAT1 activation in HaCaT cells. *Biochem Biophys Res Commun.* 2012;417(4):1254-9.
96. Kaltschmidt B, Greiner JFW, Kadhim HM, Kaltschmidt C. Subunit-Specific Role of NF-kappaB in Cancer. *Biomedicines.* 2018;6(2).
97. Lalle G, Twardowski J, Grinberg-Bleyer Y. NF-kappaB in Cancer Immunity: Friend or Foe? *Cells.* 2021;10(2).
98. Iellem A, Colantonio L, Bhakta S, Sozzani S, Mantovani A, Sinigaglia F, et al. Inhibition by IL-12 and IFN-alpha of I-309 and macrophage-derived chemokine production upon TCR triggering of human Th1 cells. *Eur J Immunol.* 2000;30(4):1030-9.
99. Chan MP, Onji M, Fukui R, Kawane K, Shibata T, Saitoh S, et al. DNase II-dependent DNA digestion is required for DNA sensing by TLR9. *Nat Commun.* 2015;6:5853.
100. Miyake K, Shibata T, Ohto U, Shimizu T, Saitoh SI, Fukui R, et al. Mechanisms controlling nucleic acid-sensing Toll-like receptors. *Int Immunol.* 2018;30(2):43-51.
101. Peters RT, Liao SM, Maniatis T. IKKepsilon is part of a novel PMA-inducible I kappa B kinase complex. *Mol Cell.* 2000;5(3):513-22.
102. Lin R, Heylbroeck C, Pitha PM, Hiscott J. Virus-dependent phosphorylation of the IRF-3 transcription factor regulates nuclear translocation, transactivation potential, and proteasome-mediated degradation. *Mol Cell Biol.* 1998;18(5):2986-96.

103. Lin R, Mamane Y, Hiscott J. Structural and functional analysis of interferon regulatory factor 3: localization of the transactivation and autoinhibitory domains. *Mol Cell Biol.* 1999;19(4):2465-74.
104. Panne D, McWhirter SM, Maniatis T, Harrison SC. Interferon regulatory factor 3 is regulated by a dual phosphorylation-dependent switch. *J Biol Chem.* 2007;282(31):22816-22.
105. Schwanke H, Stempel M, Brinkmann MM. Of Keeping and Tipping the Balance: Host Regulation and Viral Modulation of IRF3-Dependent IFNB1 Expression. *Viruses.* 2020;12(7).
106. An X, Zhu Y, Zheng T, Wang G, Zhang M, Li J, et al. An Analysis of the Expression and Association with Immune Cell Infiltration of the cGAS/STING Pathway in Pan-Cancer. *Mol Ther Nucleic Acids.* 2019;14:80-9.
107. Wu J, Leng X, Pan Z, Xu L, Zhang H. Overexpression of IRF3 Predicts Poor Prognosis in Clear Cell Renal Cell Carcinoma. *Int J Gen Med.* 2021;14:5675-92.
108. Yanai H, Chiba S, Hangai S, Kometani K, Inoue A, Kimura Y, et al. Revisiting the role of IRF3 in inflammation and immunity by conditional and specifically targeted gene ablation in mice. *Proc Natl Acad Sci U S A.* 2018;115(20):5253-8.
109. Li Y, Wilson HL, Kiss-Toth E. Regulating STING in health and disease. *J Inflamm (Lond).* 2017;14:11.
110. Konno H, Konno K, Barber GN. Cyclic dinucleotides trigger ULK1 (ATG1) phosphorylation of STING to prevent sustained innate immune signaling. *Cell.* 2013;155(3):688-98.
111. Liu Y, Mi Y, Mueller T, Kreibich S, Williams EG, Van Drogen A, et al. Multi-omic measurements of heterogeneity in HeLa cells across laboratories. *Nat Biotechnol.* 2019;37(3):314-22.
112. Cantell K. Production and action of interferon in HeLa cells. *Arch Gesamte Virusforsch.* 1961;10:510-21.
113. Blach-Olszewska Z, Halasa J, Matej H, Cembrzynska-Nowak M. Why HeLa cells do not produce interferon? *Arch Immunol Ther Exp (Warsz).* 1977;25(5):683-91.
114. Lau L, Gray EE, Brunette RL, Stetson DB. DNA tumor virus oncogenes antagonize the cGAS-STING DNA-sensing pathway. *Science.* 2015;350(6260):568-71.
115. Fujii-Maeda S, Kajiwara K, Ikizawa K, Shinazawa M, Yu B, Koga T, et al. Reciprocal regulation of thymus and activation-regulated chemokine/macrophage-derived chemokine production by interleukin (IL)-4/IL-13 and interferon-gamma in HaCaT keratinocytes is mediated by alternations in E-cadherin distribution. *J Invest Dermatol.* 2004;122(1):20-8.
116. Horikawa T, Nakayama T, Hikita I, Yamada H, Fujisawa R, Bito T, et al. IFN-gamma-inducible expression of thymus and activation-regulated chemokine/CCL17 and macrophage-derived chemokine/CCL22 in epidermal keratinocytes and their roles in atopic dermatitis. *Int Immunol.* 2002;14(7):767-73.
117. Xiao T, Kagami S, Saeki H, Sugaya M, Kakinuma T, Fujita H, et al. Both IL-4 and IL-13 inhibit the TNF-alpha and IFN-gamma enhanced MDC production in a human keratinocyte cell line, HaCaT cells. *J Dermatol Sci.* 2003;31(2):111-7.

118. Fukuda K, Fujitsu Y, Seki K, Kumagai N, Nishida T. Differential expression of thymus- and activation-regulated chemokine (CCL17) and macrophage-derived chemokine (CCL22) by human fibroblasts from cornea, skin, and lung. *J Allergy Clin Immunol.* 2003;111(3):520-6.
119. Faffe DS, Whitehead T, Moore PE, Baraldo S, Flynt L, Bourgeois K, et al. IL-13 and IL-4 promote TARC release in human airway smooth muscle cells: role of IL-4 receptor genotype. *Am J Physiol Lung Cell Mol Physiol.* 2003;285(4):L907-14.
120. Bonecchi R, Sozzani S, Stine JT, Luini W, D'Amico G, Allavena P, et al. Divergent effects of interleukin-4 and interferon-gamma on macrophage-derived chemokine production: an amplification circuit of polarized T helper 2 responses. *Blood.* 1998;92(8):2668-71.
121. Galli G, Chantry D, Annunziato F, Romagnani P, Cosmi L, Lazzeri E, et al. Macrophage-derived chemokine production by activated human T cells in vitro and in vivo: preferential association with the production of type 2 cytokines. *Eur J Immunol.* 2000;30(1):204-10.
122. Ashino S, Wakita D, Zhang Y, Chamoto K, Kitamura H, Nishimura T. CpG-ODN inhibits airway inflammation at effector phase through down-regulation of antigen-specific Th2-cell migration into lung. *Int Immunol.* 2008;20(2):259-66.
123. Wågsäter D, Dienus O, Löfgren S, Hugander A, Dimberg J. Quantification of the chemokines CCL17 and CCL22 in human colorectal adenocarcinomas. *Mol Med Rep.* 2008;1(2):211-7.
124. Menetrier-Caux C, Faget J, Biota C, Gobert M, Blay JY, Caux C. Innate immune recognition of breast tumor cells mediates CCL22 secretion favoring Treg recruitment within tumor environment. *Oncoimmunology.* 2012;1(5):759-61.
125. Yang P, Li QJ, Feng Y, Zhang Y, Markowitz GJ, Ning S, et al. TGF- β -miR-34a-CCL22 signaling-induced Treg cell recruitment promotes venous metastases of HBV-positive hepatocellular carcinoma. *Cancer Cell.* 2012;22(3):291-303.
126. Hino R, Kobayashi M, Mori T, Orimo H, Shimauchi T, Kabashima K, et al. Inhibition of T helper 2 chemokine production by narrowband ultraviolet B in cultured keratinocytes. *Br J Dermatol.* 2007;156(5):830-7.
127. Ni H, Zhang H, Li L, Huang H, Guo H, Zhang L, et al. T cell-intrinsic STING signaling promotes regulatory T cell induction and immunosuppression by upregulating FOXP3 transcription in cervical cancer. *J Immunother Cancer.* 2022;10(9).
128. Capper D, von Deimling A, Brandes AA, Carpentier AF, Kesari S, Sepulveda-Sanchez JM, et al. Biomarker and Histopathology Evaluation of Patients with Recurrent Glioblastoma Treated with Galunisertib, Lomustine, or the Combination of Galunisertib and Lomustine. *Int J Mol Sci.* 2017;18(5).
129. Donlon NE, Sheppard A, Davern M, O'Connell F, Phelan JJ, Power R, et al. Linking Circulating Serum Proteins with Clinical Outcomes in Esophageal Adenocarcinoma-An Emerging Role for Chemokines. *Cancers (Basel).* 2020;12(11).
130. Freier CP, Kuhn C, Endres S, Mayr D, Friese K, Jeschke U, et al. FOXP3+ Cells Recruited by CCL22 into Breast Cancer Correlates with Less Tumor Nodal Infiltration. *Anticancer Res.* 2016;36(6):3139-45.

131. Li Y, Chen X, Li D, Yang Z, Bai Y, Hu S, et al. Identification of prognostic and therapeutic value of CC chemokines in Urothelial bladder cancer: evidence from comprehensive bioinformatic analysis. *BMC Urol.* 2021;21(1):173.
132. Nakanishi T, Imaizumi K, Hasegawa Y, Kawabe T, Hashimoto N, Okamoto M, et al. Expression of macrophage-derived chemokine (MDC)/CCL22 in human lung cancer. *Cancer Immunol Immunother.* 2006;55(11):1320-9.
133. Thomas JK, Mir H, Kapur N, Bae S, Singh S. CC chemokines are differentially expressed in Breast Cancer and are associated with disparity in overall survival. *Sci Rep.* 2019;9(1):4014.
134. Zhou M, Bracci PM, McCoy LS, Hsuang G, Wiemels JL, Rice T, et al. Serum macrophage-derived chemokine/CCL22 levels are associated with glioma risk, CD4 T cell lymphopenia and survival time. *Int J Cancer.* 2015;137(4):826-36.
135. Zhou X, Xiao C, Han T, Qiu S, Wang M, Chu J, et al. Prognostic biomarkers related to breast cancer recurrence identified based on Logit model analysis. *World J Surg Oncol.* 2020;18(1):254.
136. Han Y, Ding Z, Chen B, Liu Y, Liu Y. A Novel Inflammatory Response-Related Gene Signature Improves High-Risk Survival Prediction in Patients With Head and Neck Squamous Cell Carcinoma. *Front Genet.* 2022;13:767166.
137. Li H, Chen X, Zeng W, Zhou W, Zhou Q, Wang Z, et al. Radiation-Enhanced Expression of CCL22 in Nasopharyngeal Carcinoma is Associated With CCR4(+) CD8 T Cell Recruitment. *Int J Radiat Oncol Biol Phys.* 2020;108(1):126-39.
138. Li X, Liu Z, Zhou W, Liu X, Cao W. Downregulation of CCL22 and mutated NOTCH1 in tongue and mouth floor squamous cell carcinoma results in decreased Th2 cell recruitment and expression, predicting poor clinical outcome. *BMC Cancer.* 2021;21(1):922.
139. Chen W, Huang J, Xiong J, Fu P, Chen C, Liu Y, et al. Identification of a Tumor Microenvironment-Related Gene Signature Indicative of Disease Prognosis and Treatment Response in Colon Cancer. *Oxid Med Cell Longev.* 2021;2021:6290261.
140. Dai S, Xu S, Ye Y, Ding K. Identification of an Immune-Related Gene Signature to Improve Prognosis Prediction in Colorectal Cancer Patients. *Front Genet.* 2020;11:607009.
141. Wang H, Luo K, Guan Z, Li Z, Xiang J, Ou S, et al. Identification of the Crucial Role of CCL22 in F. nucleatum-Related Colorectal Tumorigenesis that Correlates With Tumor Microenvironment and Immune Checkpoint Therapy. *Front Genet.* 2022;13:811900.
142. Wang Y, Zhang L, Shi G, Liu M, Zhao W, Zhang Y, et al. Effects of Inflammatory Response Genes on the Immune Microenvironment in Colorectal Cancer. *Front Genet.* 2022;13:886949.
143. Wu B, Tao L, Yang D, Li W, Xu H, He Q. Development of an Immune Infiltration-Related Eight-Gene Prognostic Signature in Colorectal Cancer Microenvironment. *Biomed Res Int.* 2020;2020:2719739.
144. Zhang X, Zhao H, Shi X, Jia X, Yang Y. Identification and validation of an immune-related gene signature predictive of overall survival in colon cancer. *Aging (Albany NY).* 2020;12(24):26095-120.
145. Cohen EEW, Pishvaian MJ, Shepard DR, Wang D, Weiss J, Johnson ML, et al. A phase Ib study of utomilumab (PF-05082566) in combination with mogamulizumab in patients with advanced solid

- tumors. *J Immunother Cancer*. 2019;7(1):342.
146. Doi T, Muro K, Ishii H, Kato T, Tsushima T, Takenoyama M, et al. A Phase I Study of the Anti-CC Chemokine Receptor 4 Antibody, Mogamulizumab, in Combination with Nivolumab in Patients with Advanced or Metastatic Solid Tumors. *Clinical cancer research : an official journal of the American Association for Cancer Research*. 2019;25(22):6614-22.
 147. Zamarin D, Hamid O, Nayak-Kapoor A, Sahebjam S, Sznol M, Collaku A, et al. Mogamulizumab in Combination with Durvalumab or Tremelimumab in Patients with Advanced Solid Tumors: A Phase I Study. *Clinical cancer research : an official journal of the American Association for Cancer Research*. 2020;26(17):4531-41.
 148. Zhang T, Sun J, Li J, Zhao Y, Zhang T, Yang R, et al. Safety and efficacy profile of mogamulizumab (Poteligeo) in the treatment of cancers: an update evidence from 14 studies. *BMC Cancer*. 2021;21(1):618.
 149. Chang DK, Sui J, Geng S, Muvaffak A, Bai M, Fuhlbrigge RC, et al. Humanization of an anti-CCR4 antibody that kills cutaneous T-cell lymphoma cells and abrogates suppression by T-regulatory cells. *Mol Cancer Ther*. 2012;11(11):2451-61.
 150. Ogura M, Ishida T, Hatake K, Taniwaki M, Ando K, Tobinai K, et al. Multicenter phase II study of mogamulizumab (KW-0761), a defucosylated anti-cc chemokine receptor 4 antibody, in patients with relapsed peripheral T-cell lymphoma and cutaneous T-cell lymphoma. *J Clin Oncol*. 2014;32(11):1157-63.
 151. Jackson JJ, Ketcham JM, Younai A, Abraham B, Biannic B, Beck HP, et al. Discovery of a Potent and Selective CCR4 Antagonist That Inhibits T(reg) Trafficking into the Tumor Microenvironment. *J Med Chem*. 2019;62(13):6190-213.
 152. Santulli-Marotto S, Wheeler J, Lacy ER, Boakye K, Luongo J, Wu SJ, et al. CCL22-specific Antibodies Reveal That Engagement of Two Distinct Binding Domains on CCL22 Is Required for CCR4-mediated Function. *Monoclon Antib Immunodiagn Immunother*. 2015;34(6):373-80.
 153. Zhu J, Smith K, Hsieh PN, Mburu YK, Chattopadhyay S, Sen GC, et al. High-throughput screening for TLR3-IFN regulatory factor 3 signaling pathway modulators identifies several antipsychotic drugs as TLR inhibitors. *J Immunol*. 2010;184(10):5768-76.
 154. Cook PR, Jones CE, Furano AV. Phosphorylation of ORF1p is required for L1 retrotransposition. *Proc Natl Acad Sci U S A*. 2015;112(14):4298-303.
 155. Maddalo D, Manchado E, Concepcion CP, Bonetti C, Vidigal JA, Han YC, et al. In vivo engineering of oncogenic chromosomal rearrangements with the CRISPR/Cas9 system. *Nature*. 2014;516(7531):423-7.
 156. Park J, Bae S, Kim JS. Cas-Designer: a web-based tool for choice of CRISPR-Cas9 target sites. *Bioinformatics*. 2015;31(24):4014-6.
 157. Bae S, Park J, Kim JS. Cas-OFFinder: a fast and versatile algorithm that searches for potential off-target sites of Cas9 RNA-guided endonucleases. *Bioinformatics*. 2014;30(10):1473-5.

Figures

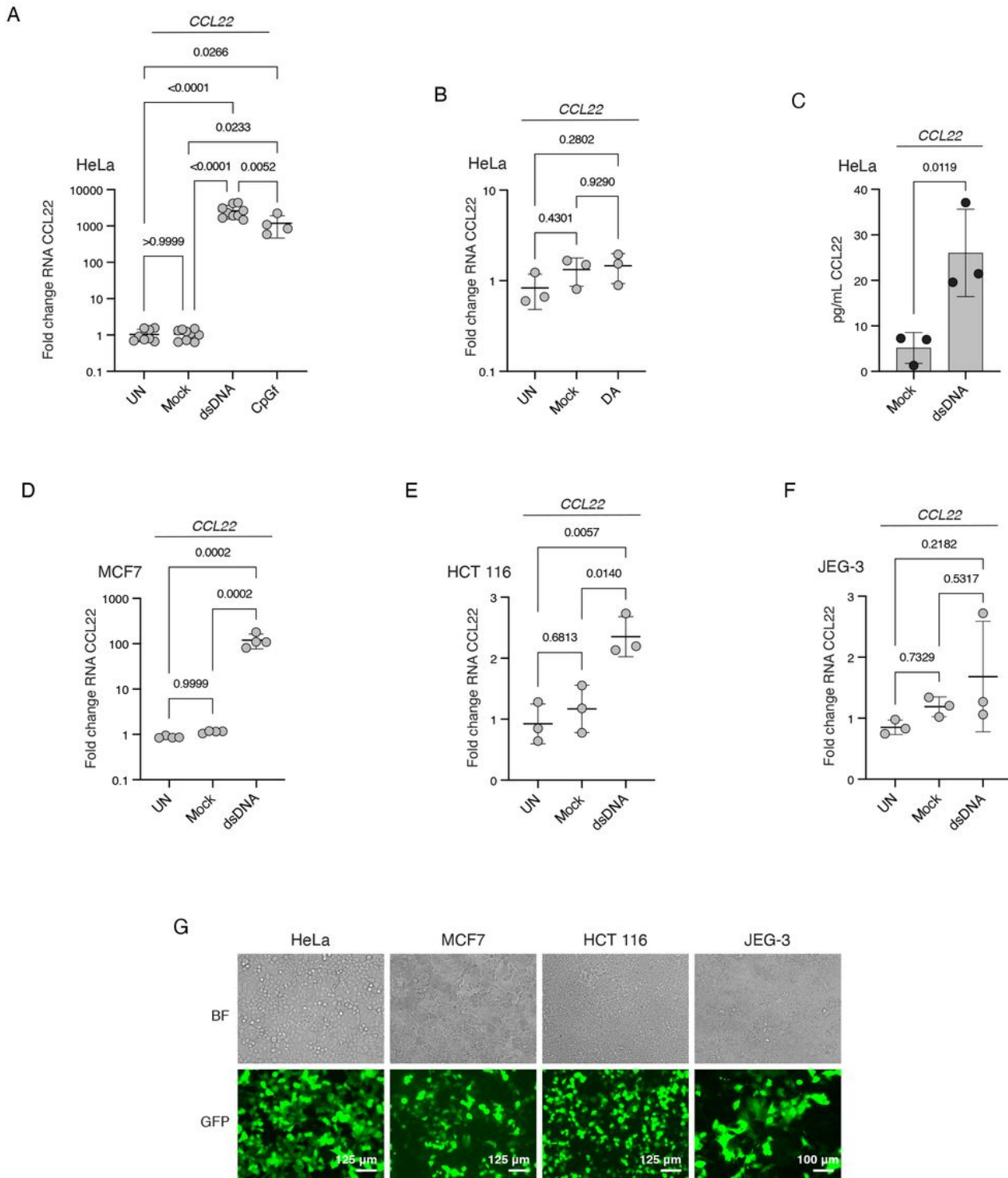


Figure 1

dsDNA increases CCL22 in epithelial cancer cells. (A) HeLa cells were untreated (UN) or treated with a mock control (TransIT-LT1 transfection reagent only), dsDNA (2 μ g/mL), or CpG-free (CpGf) dsDNA (2 μ g/mL), each transfected with TransIT-LT1 at a 1:2 ratio and harvested 48 hours after transfection.

Resulting levels of CCL22 mRNA are shown. Each data point represents an independent experiment. Significance testing was performed with a one-way ANOVA and Tukey's pairwise comparison; error bars represent standard deviations. (B) HeLa cells were untreated (UN) or treated with a mock control (TransIT-LT1 transfection reagent only) or a reaction containing dsDNA (2 $\mu\text{g}/\text{mL}$) alone (DA) without transfection reagent and harvested 48 hours after treatment. Resulting levels of CCL22 mRNA are shown with DA relative to the average of UN, Mock. Each data point represents an independent experiment. Significance testing was performed with a one-way ANOVA and Tukey's pairwise comparison; error bars represent standard deviations. (C) HeLa cells were seeded at approximately 4×10^5 cells in 2 mL total volume and treated with dsDNA 24 hours after plating as in (A). Media was harvested 48 hours after treatment, spun down to remove any cell debris, and used fresh for each independent ELISA. Absorbance values for technical replicates were averaged and final concentrations of samples were determined from the best-fit straight line of log-log plotted standard curve data in PRISM. Results shown are from three independent experiments. Significance testing was performed with an unpaired, one-tailed t test; error bars represent standard deviations. (D-F) MCF7 (D), HCT 116 (E), and JEG-3 (F) cells were untreated (UN) or treated with a mock control (indicated transfection reagent only) or dsDNA (2 $\mu\text{g}/\text{mL}$) using TransfeX at a 1:4 ratio (MCF7) or TransIT-LT1 (HCT 116, 1:4 ratio; JEG-3, 1:3 ratio). Cells were harvested 48 hours after transfection. Resulting levels of CCL22 mRNA are shown. Each data point represents an independent experiment. Significance testing was performed with a one-way ANOVA and Tukey's pairwise comparison; error bars represent standard deviations. (G) Cells were transfected as described above in parallel experiments using a GFP expression plasmid (2 $\mu\text{g}/\text{mL}$ with transfection reagents and ratios indicated in (A, D-F) and imaged 48 hours after transfection. Brightfield (BF) shows the confluency of cells in the same field of view as GFP.

cGAM(PS)2(Rp/Sp) with TransIT-LT1 at a 1:1 $\mu\text{g}/\mu\text{L}$ ratio or a mock control for the 10 μM 2'3'-cGAM(PS)2(Rp/Sp) sample, which contained the largest volume of transfection reagent, and harvested 24 hours post transfection for RTqPCR. Resulting levels of CCL22 are shown relative to untreated cells. Each data point represents an independent experiment. Significance testing was performed with a one-way ANOVA and Dunnett's multiple comparison test; error bars represent standard deviations. (C) MCF7 cells were transfected with a mock control or 10 μM 2'3'-cGAM(PS)2(Rp/Sp) with TransfeX at a 1:2 $\mu\text{g}/\mu\text{L}$ ratio and harvested 24 hours post transfection for RTqPCR. Resulting fold change of CCL22 is shown relative to untreated cells. Each data point represents an independent experiment. Significance testing was performed with an unpaired one-tailed t test; error bars represent standard deviations. (D) HeLa cells were transfected with a mock control or indicated concentrations of 2'3'-cGAM(PS)2(Rp/Sp) with TransIT-LT1 at a 1:1 $\mu\text{g}/\mu\text{L}$ ratio and harvested at indicated timepoints. Lysates (60 μg) and THP-1 positive control (15 μg) were resolved with SDS-PAGE and probed for phospho-STING and beta-tubulin. The image shown is representative of at least three independent experiments. (E) Diagram shows the bases of *TMEM173* targeted for deletion by CRISPR-Cas9, with gRNA binding sites in red and PAM sequences underlined. The expected deletions for KO-1 and KO-2 are 190 bp and 394 bp, respectively. Illustration was generated by BioRender.com. (F) Genomic DNA of unedited (WT) and monoclonal KO-1 and KO-2 cell lines was extracted and amplified using primers flanking the intended *TMEM173* deletions, TMEM-F and TMEM-R. Separation with agarose electrophoresis revealed the expected amplicon sizes for unedited (unedited WT, 874 bp), KO-1 (~684 bp) and KO-2 (~480 bp). (G) Whole cell lysates (25 μg) from unedited (WT), KO-1, and KO-2 cells were resolved with SDS-PAGE and probed for STING and beta-tubulin. The image shown is representative of at least three independent experiments. (H) Unedited (WT), KO-1, and KO-2 HeLa cells were untreated or transfected with a mock control or dsDNA (2 $\mu\text{g}/\text{mL}$) with TransIT-LT1 at a 1:2 ratio and harvested after 48 hours for RTqPCR. Resulting fold change of CCL22 mRNA is shown relative to the average of untreated and mock controls for each cell line. Each data point represents an independent experiment. Significance testing was performed with a one-way ANOVA and Tukey's pairwise comparison of each knockout cell line to unedited (WT) cells; error bars represent standard deviations. (I) Parallel experiments with a GFP expression plasmid (2 $\mu\text{g}/\text{mL}$, TransIT-LT1 1:2 ratio) show that DNA is effectively incorporated into STING knock out cells. Cells were imaged 48 hours post transfection. Brightfield (BF) shows the confluency of cells in the same field of view as GFP.

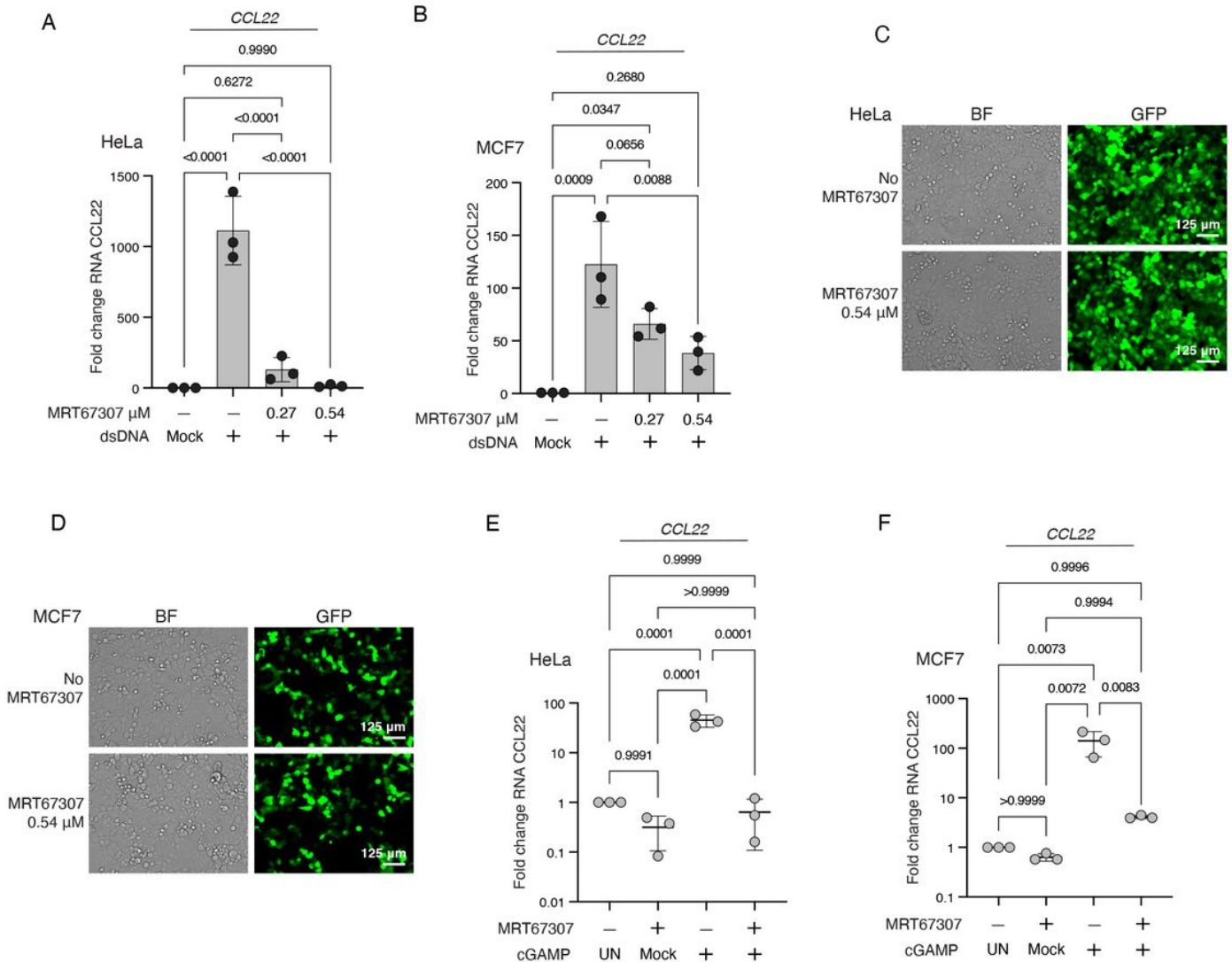


Figure 3

STING agonist 2'3'-cGAM(PS)2(Rp/Sp) and dsDNA upregulates CCL22 in a manner dependent on TBK1/IKK ϵ . (A) HeLa cells were seeded in 12-well plates to achieve approximately 65% confluency in 24 hours then treated with either the TBK1/IKK ϵ inhibitor MRT67307 at concentrations indicated in the figure or a water vehicle control for approximately 1.5 hours prior to transfection with a mock control or dsDNA (2 μ g/mL) with TransIT-LT1 at a 1:2 ratio. Cells were harvested 48 hours after transfection for RTqPCR. Resulting levels of CCL22 mRNA are shown. Each data point represents an independent experiment. Significance testing was performed with a one-way ANOVA and Tukey's pairwise comparison; error bars represent standard deviations. (B) MCF7 cells were seeded in 12-well plates to achieve approximately 50% confluency in 24 hours, then cells were treated with either the TBK1/IKK ϵ inhibitor MRT67307 at concentrations indicated in the figure or a water vehicle control for approximately 1.5 hours prior to transfection with a mock control or dsDNA (2 μ g/mL) with TransfeX at a 1:4 ratio. Cells were harvested, processed, and data analyzed as in (A). (C-D) HeLa cells (C) and MCF7 cells (D) were treated with MRT67307 as described in (A-B) then transfected in parallel experiments using a GFP expression plasmid

(2 $\mu\text{g}/\text{mL}$, TransIT-LT1 1:2 ratio for HeLa and TransfeX at 1:4 ratio for MCF7) and imaged 48 hours after transfection. Brightfield (BF) shows the confluency of cells in the same field of view as GFP. (E-F) HeLa cells (E) and MCF7 cells (F) were treated with 0.54 μM of the TBK1/IKK ϵ inhibitor MRT67307 or a water vehicle control for approximately 1.5 hours prior to no treatment (UN) or transfection with mock controls or 10 μM 2'3'-cGAM(PS)2(Rp/Sp) using TransIT-LT1 at a 1:1 $\mu\text{g}/\mu\text{L}$ ratio (HeLa) or TransfeX at a 1:2 $\mu\text{g}/\mu\text{L}$ ratio (MCF7). Cells were harvested 24 hours after transfection. Resulting fold change of CCL22 is shown. Each data point represents an independent experiment. Significance testing was performed with a one-way ANOVA and Tukey's pairwise comparison; error bars represent standard deviations.

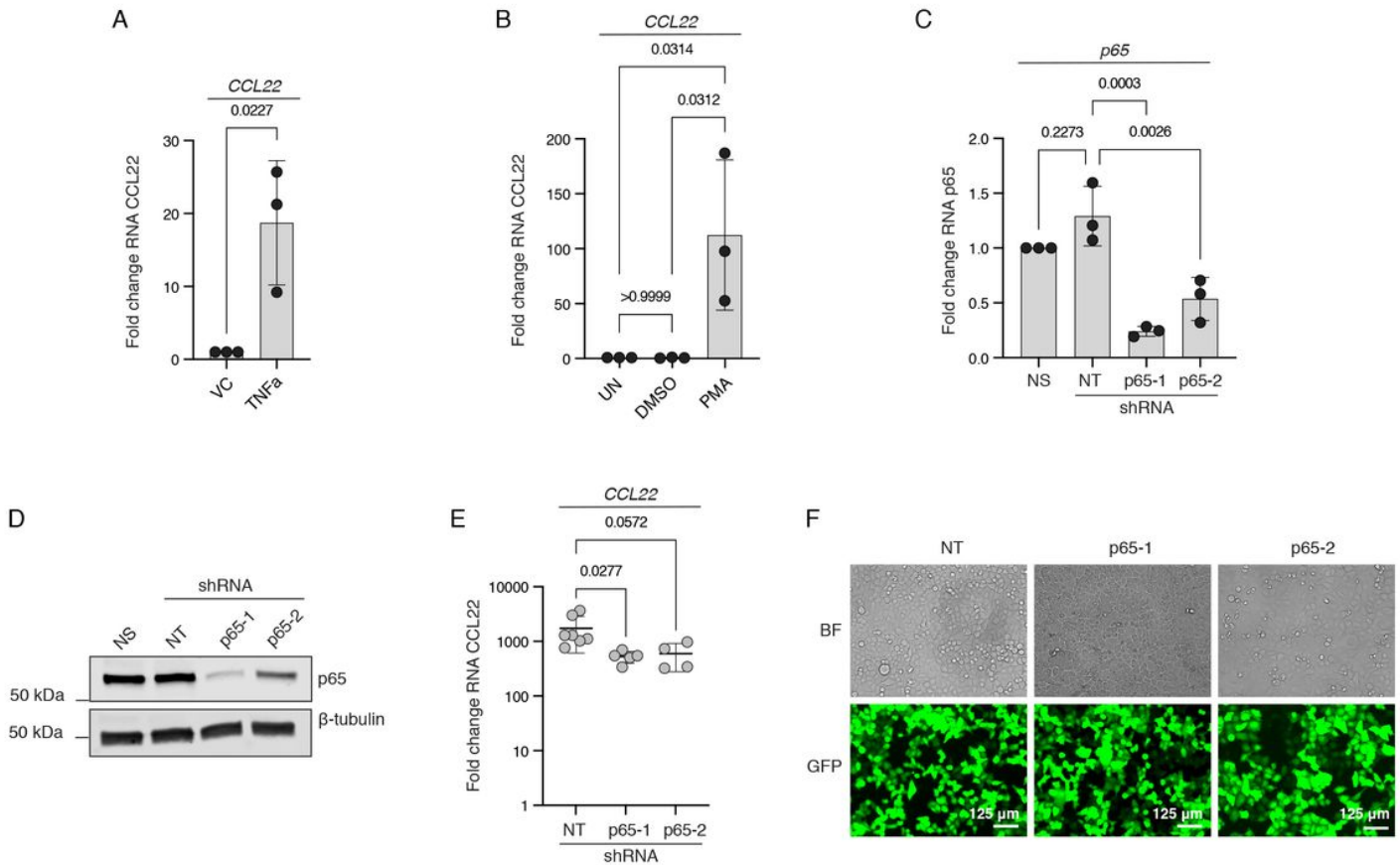


Figure 4

NF- κ B contributes minimally to CCL22 upregulation by dsDNA. (A) HeLa cells were seeded in 12-well plates to achieve approximately 65% confluency in 24 hours, at which time cells were treated with either 8 ng/mL TNF α or a water vehicle control (VC). Cells were harvested 24 hours after treatment, and RTqPCR was performed. Resulting levels of CCL22 mRNA are shown. Each data point represents an independent experiment. Significance testing was performed with an unpaired, two-tail t test; error bars represent standard deviations. (B) HeLa cells were seeded and grown as for (A) and either untreated (UN) or treated with 10 ng/mL PMA or a 0.0004% DMSO vehicle control. Significance testing was performed with a one-way ANOVA and Tukey's pairwise comparison; error bars represent standard deviations. (C) HeLa cells expressing no shRNA (NS) or stably expressing a non-targeting shRNA (NT) or shRNAs against RELA/p65

(p65-1 or p65-2) were harvested for RTqPCR; levels of RELA/p65 RNA are shown relative to NS. Each data point represents an independent experiment. Significance testing was performed with a one-way ANOVA and Tukey's pairwise comparison; error bars represent standard deviations. (D) Lysates (20 μ g) from HeLa cells expressing no shRNA (NS) or stably expressing either non-targeting shRNA (NT) or shRNAs against RELA/p65 (p65-1 or p65-2) were resolved using SDS-PAGE and probed for RELA/p65 and beta-tubulin. The image shown is representative of at least three independent experiments. (E) HeLa cells described in (C) and (D) were transfected with a mock control or dsDNA (2 μ g/mL) with TransIT-LT1 at a 1:2 ratio and harvested after 48 hours for RTqPCR. Resulting fold change of CCL22 mRNA is shown relative to the mock control for each cell line. Each data point represents an independent experiment. Significance testing was performed with a one-way ANOVA and Dunnett's pairwise comparison of each shRNA group to the control non-targeting (NT) group; note that this analysis was performed alongside the IRF3 shRNA groups from Figure 6C in order that all non-targeting control experiments be included; error bars represent standard deviations. (F) HeLa cells carrying the shRNAs described above were transfected as in (E) in parallel experiments using a GFP expression plasmid (2 μ g/mL, TransIT-LT1 1:2 ratio) and imaged 48 hours after transfection. Brightfield (BF) shows the confluency of cells in the same field of view as GFP.

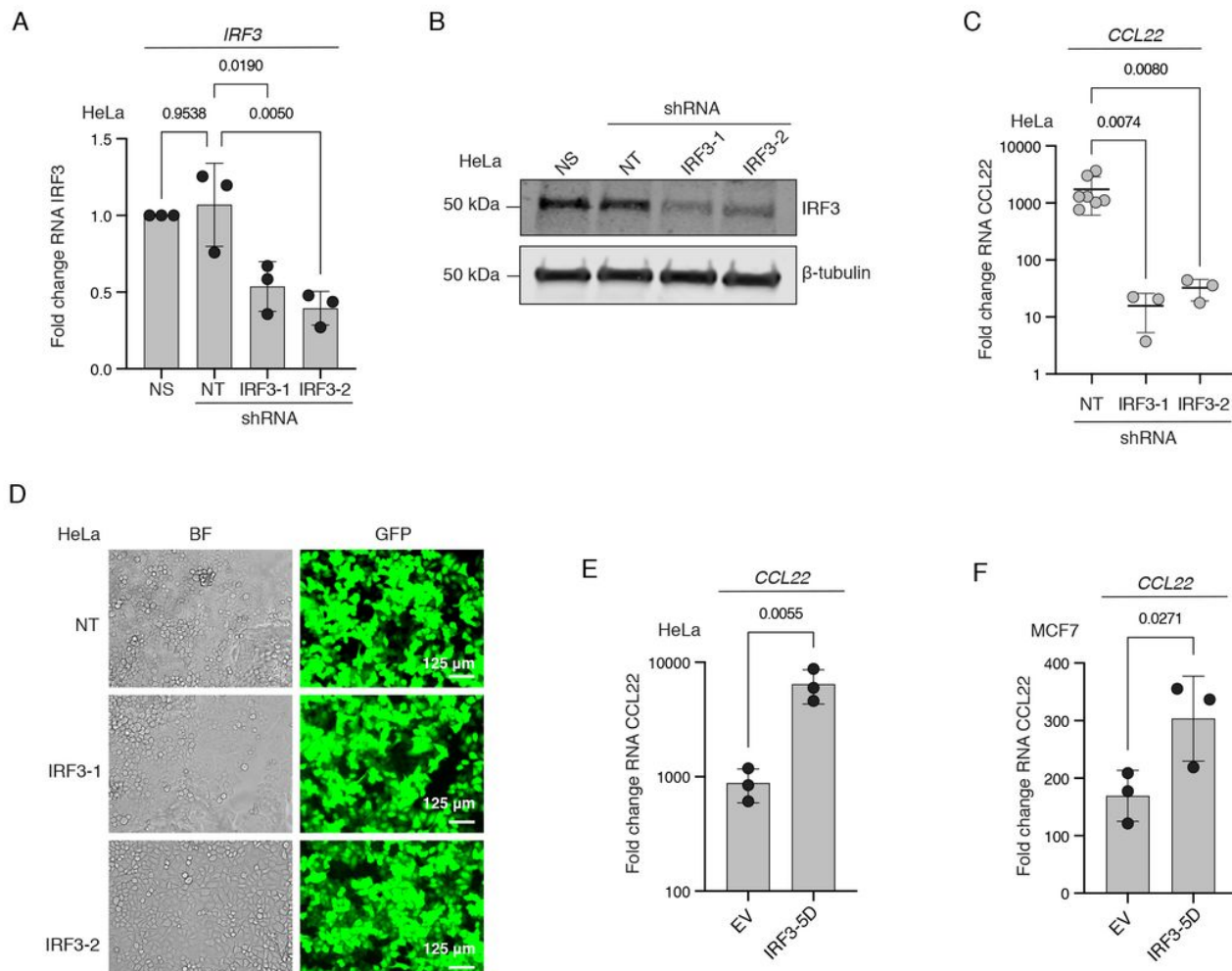


Figure 5

IRF3 is indispensable for CCL22 upregulation in response to dsDNA. (A) HeLa cells expressing no shRNA (NS) or stably expressing a non-targeting shRNA (NT) or shRNAs against IRF3 (IRF3-1 or IRF3-2) were harvested for RTqPCR; levels of IRF3 RNA are shown relative to NS. Each data point represents an independent experiment. Significance testing was performed with a one-way ANOVA and Tukey's pairwise comparison; error bars represent standard deviations. (B) Lysates (20 μ g) from HeLa cells carrying no shRNA (NS), non-targeting shRNA (NT) or shRNAs against IRF3 (IRF3-1 or IRF3-2) were resolved using SDS-PAGE and probed for IRF3 and beta-tubulin. The image shown is representative of at least three independent experiments. (C) HeLa cells described in (A) and (B) were transfected with a mock control or dsDNA (2 μ g/mL) with TransIT-LT1 at a 1:2 ratio and harvested after 48 hours for RTqPCR. Resulting fold change of CCL22 mRNA is shown relative to the mock control for each cell line. Each data point represents an independent experiment. Significance testing was performed with a one-way ANOVA and Dunnett's pairwise comparison of each shRNA group to the control non-targeting group; note that this analysis was performed alongside the RELA/p65 shRNA groups from Figure 5E in order that all non-targeting control experiments be included; error bars represent standard deviations. (D) HeLa cells stably expressing the shRNAs described above were transfected as in (C) in parallel experiments using a GFP expression plasmid (2 μ g/mL, TransIT-LT1, 1:2 ratio) and imaged 48 hours after transfection. Brightfield (BF) shows the confluency of cells in the same field of view as GFP. (E) HeLa cells and (F) MCF7 cells were transfected with a mock control or 2 μ g/mL of empty plasmid (EV) or the constitutively active IRF3-5D with TransIT-LT1 at a 1:2 ratio (HeLa) or TransfeX at a 1:4 ratio (MCF7). Cells were harvested 48 hours after transfection. Fold change of CCL22 mRNA in EV and IRF3-5D treated samples is shown relative to the mock control. Each data point represents an independent experiment. Significance testing was performed with an unpaired, one-tailed t test; error bars represent standard deviations.

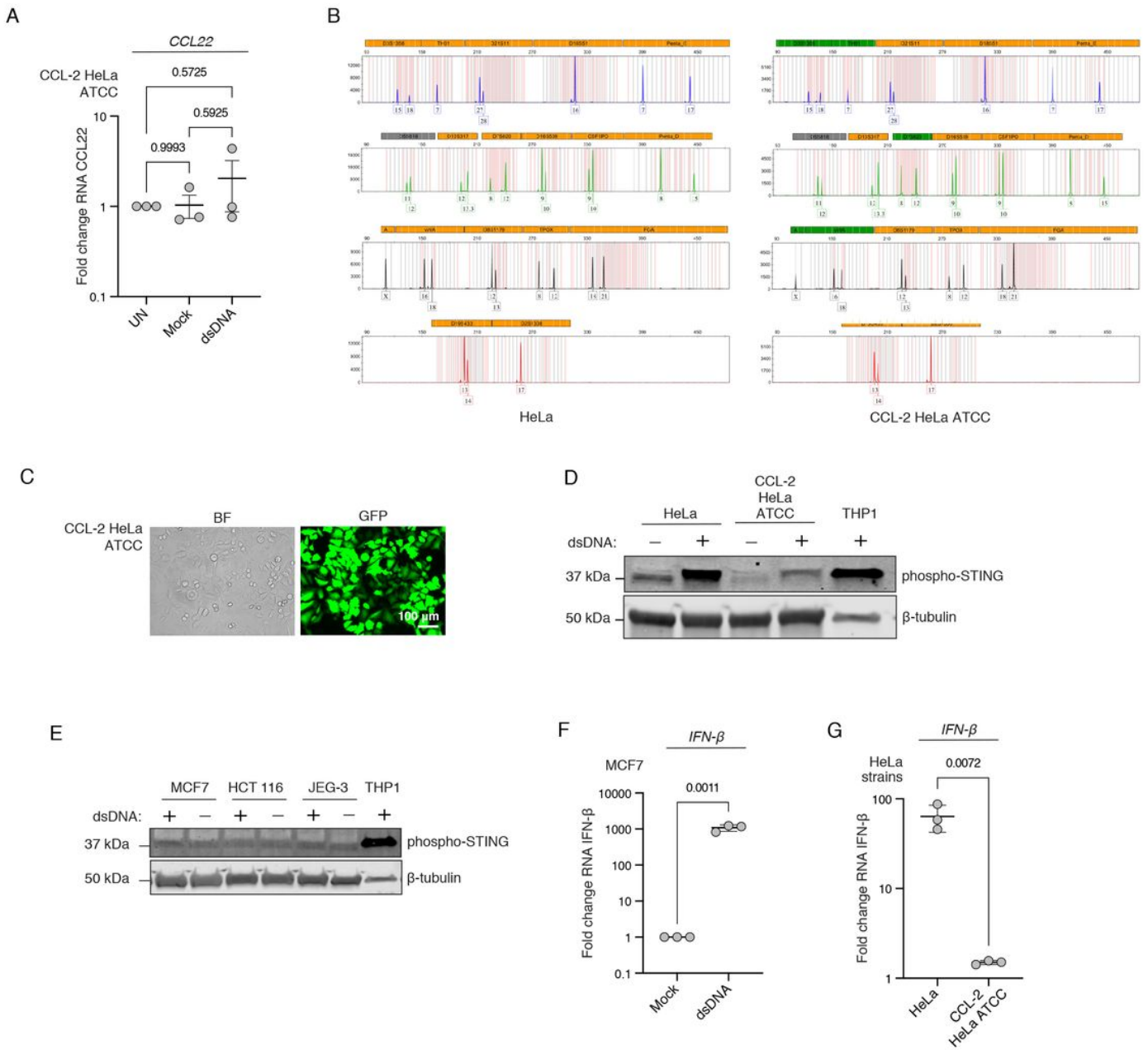


Figure 6

Two strains of HeLa cells differ dramatically in upregulation of CCL22 by dsDNA. (A) CCL-2 HeLa cells from ATCC were untreated or transfected with a mock control or dsDNA (2 μ g/mL) with TransIT-LT1 at a 1:2 ratio and harvested after 48 hours for RTqPCR. Resulting fold change of CCL22 mRNA is shown. Each data point represents an independent experiment. Significance testing was performed with a one-way ANOVA and Tukey's pairwise comparison; error bars represent standard deviations. (B) Samples of our original HeLa cell line and CCL-2 HeLa cells from ATCC were each sent to ATCC for authentication with STR profile analysis. Results are shown side-by-side. (C) CCL-2 HeLa cells from ATCC were transfected as in (A) in parallel experiments using a GFP expression plasmid (2 μ g/mL, TransIT-LT1, 1:2 ratio) and imaged 48 hours after transfection. Brightfield (BF) shows the confluency of cells in the same field of

view as GFP. (D) Indicated cell lines were transfected as described in (A) and harvested after 48 hours. Lysates (60 μ g) and THP-1 positive control (15 μ g) were separated with SDS-PAGE and probed for phospho-STING (S366) and beta-tubulin. The image shown is representative of at least three independent experiments. (E) Indicated cells were untreated or transfected with dsDNA (2 μ g/mL) using TransfeX at a 1:4 ratio (MCF7) or TransIT-LT1 (HCT 116, 1:4 ratio; JEG-3, 1:3 ratio). Cells were harvested 48 hours after transfection. Lysates (60 μ g) and THP1 positive control (15 μ g) were separated with SDS-PAGE and probed for phospho-STING (S366) and beta-tubulin. The image shown is representative of at least three independent experiments. (F) MCF7 cells were treated with mock reactions or dsDNA (2 μ g/mL) using TransfeX at a 1:4 ratio and harvested after 48 hours for RTqPCR. Resulting fold change of IFN- β mRNA is shown. Each data point represents an independent experiment. Significance testing was performed with an unpaired two-tailed t test; error bars represent standard deviations. (G) HeLa cell strains were untreated or transfected with a mock control or dsDNA (2 μ g/mL) with TransIT-LT1 at a 1:2 ratio and harvested after 48 hours for RTqPCR. Resulting fold change of IFN- β mRNA relative to the untreated and mock controls is shown for each cell line. Significance testing was performed with an unpaired two-tailed t test; error bars represent standard deviations.

Supplementary Files

This is a list of supplementary files associated with this preprint. Click to download.

- [Datasourcefile20221111.xlsx](#)
- [Fig.S120221101.pdf](#)